

Manuscript prepared for Geosci. Model Dev.  
with version 2014/09/16 7.15 Copernicus papers of the L<sup>A</sup>T<sub>E</sub>X class copernicus.cls.  
Date: 23 August 2015

# Addressing the Challenge of Nonphysical Solution Negativity in Coupling a Reactive Transport Model with a Global Land Surface Model for Mechanistic Biogeochemistry Representation

Guoping Tang<sup>1</sup>, Fengming Yuan<sup>1</sup>, Gautam Bisht<sup>1,2</sup>, Glenn E. Hammond<sup>3</sup>, Peter C. Lichtner<sup>4</sup>, Jitendra Kumar<sup>1</sup>, Richard T. Mills<sup>1,5</sup>, Xiaofeng Xu<sup>1,6</sup>, Ben Andre<sup>7</sup>, Forrest M. Hoffman<sup>1</sup>, Scott L. Painter<sup>1</sup>, and Peter E. Thornton<sup>1</sup>

<sup>1</sup>Oak Ridge National Laboratory, Oak Ridge, Tennessee, United States

<sup>2</sup>Lawrence Berkeley National Laboratory, Berkeley, California, United States

<sup>3</sup>Sandia National Laboratories, Albuquerque, New Mexico, United States

<sup>4</sup>OFM Research, Redmond, Washington, United States

<sup>5</sup>Intel Incorporation, Portland, Oregon, United States

<sup>6</sup>University of Texas at El Paso, El Paso, Texas, United States

<sup>7</sup>National Center for Atmospheric Research, Boulder, Colorado, United States

*Correspondence to:* Peter E. Thornton (thorntonpe@ornl.gov)

This manuscript has been authored by UT-Battelle, LLC under Contract No. DE-AC05-00OR22725 with the U.S. Department of Energy. The United States Government retains and the publisher, by accepting the article for publication, acknowledges that the United States Government retains a non-exclusive, paid-up, irrevocable, world-wide license to publish or reproduce the published form of

- 5 this manuscript, or allow others to do so, for United States Government purposes. The Department of Energy will provide public access to these results of federally sponsored research in accordance with the DOE Public Access Plan(<http://energy.gov/downloads/doe-public-access-plan>).

**Abstract.** Reactive transport codes (e.g., PFLOTRAN) are increasingly used to improve the representation of biogeochemical processes in terrestrial ecosystem models (e.g., the Community Land Model, CLM). As CLM and PFLOTRAN use explicit and implicit time stepping, respectively, implementation of CLM biogeochemical reactions in PFLOTRAN can result in negative primary species concentrations, which is not physically meaningful. The objective of this work is to address the non-physical solution negativity to obtain accurate, efficient, and robust solutions. We illustrate the implementation of a reaction network with the CLM-CN decomposition, nitrification, denitrification, and plant nitrogen uptake reactions and test the implementation at arctic, temperate, and tropical sites. We examine use of scaling back the update during each iteration (SU), log transformation (LT), and downregulating the reaction rate to account for reactant availability limitation to enforce nonnegativity. Both SU and LT guarantee nonnegativity. When a very small scaling factor occurs due to either consumption or numerical overshoot, and the iterations are deemed converged because of too small an update, SU can introduce excessive numerical error. LT involves multiplication of the Jacobian matrix by the concentration vector, which increases the condition number, decreases the time step size, and increases the computational cost. Neither SU nor LT prevents zero concentration. When the concentration is close to machine precision or zero, a small positive update stops all reactions for SU, and LT can fail due to a singular Jacobian matrix. The consumption rate has to be downregulated such that the solution to the mathematical representation is positive. A first-order rate downregulates consumption and is nonnegative, and adding a residual concentration makes it positive. For zero-order rate (the reaction rate is not a function of a reactant), representing the availability limitation of each reactant with a Monod substrate limiting function provides a smooth transition between a zero-order rate when the reactant is abundant and first-order rate when the reactant becomes limiting. When the half saturation is small, marching through the transition may require small time step sizes to resolve the sharp change within a small range of concentration values. Our results from simple tests and CLM-PFLOTRAN simulations caution against use of SU and indicate that accurate, stable, and relatively efficient solutions can be achieved with LT and downregulation with Monod substrate limiting function and residual concentration.

35 **1 Introduction**

Land surface models calculate the fluxes of energy, water, and green house gases across the land-atmosphere interface for the atmospheric general circulation models for climate simulation and weather forecasting (Sellers et al., 1997). Evolving from the first generation “bucket”, second generation “biophysical”, and third generation “physiological” models (Sellers et al., 1997; Seneviratne et al., 2010), current land surface models, e.g., the Community Land Model (CLM), implement comprehensive thermal, hydrological, and biogeochemical processes (Oleson et al., 2013). The important role of soil biogeochemistry is suggested by the confirmation that the increase of carbon dioxide, methane, and nitrous oxide in the atmosphere since the preindustrial time is the main driving cause of climate change, and interdependent water, carbon and nitrogen cycles in terrestrial ecosystems are very sensitive to climate changes (IPCC, 2013). CLM4.5 incorporates CLM-CN and CENTURY, and adds methane models for carbon and nitrogen cycles (Oleson et al., 2013). In addition to  $\sim 250$  soil biogeochemical models developed in the past  $\sim 80$  years (Manzoni and Porporato, 2009), increasingly mechanistic models continue to be developed to increase the fidelity of process representation for improving climate prediction (e.g., Wang et al., 2012; Riley et al., 2014).

As land surface models usually hardcode the reaction network (pools/species, reactions, rate formulae), substantial effort is often required to revise the source code for testing alternative biogeochemical models, and incorporating new process understanding. To mitigate this issue, Fang et al. (2013) demonstrates the use of a reaction-based approach to facilitate implementation of CLM-CN and CENTURY models, and incorporation of phosphorus cycle. While Fang et al. (2013) adds a reaction solver developed from the reactive transport (geochemical) model literature for algebraic and ordinary differential equations, Tang et al. (2013b) solves the advection diffusion equation in CLM using operator splitting with the Crank-Nicolson scheme for diffusion and a forward-in-time upstream discretization for advection. In contrast, a reactive transport code, TOUGH-REACT, is used to develop multi-phase (gas, aqueous, solid) mechanistic carbon and nitrogen cycle models with many speciation and microbial reactions (Maggi et al., 2008; Gu and Riley, 2010; Riley et al., 2014). Coupling a reactive transport code (e.g., Steefel et al., 2014) with CLM facilitates testing and implementation of increasingly mechanistic biogeochemical models in terrestrial ecosystem models by taking advantages of the developments in reactive transport modeling.

The nonphysical solution negativity arises in the coupling of a reactive transport code with CLM as an essential aspect of these land surface models is the ability to simulate competition for nutrients (e.g., mineral nitrogen, phosphorus, etc.) among plants and microbes. For example, the CLM-CN decomposition cascade downregulates the demand based on the available nitrogen ( $N$ ) (Oleson et al., 2013; Thornton and Rosenbloom, 2005). Specifically, marching from time step  $k$  to  $k+1$  with a supply rate  $S^k$  and consumption rate  $D^k$  using the forward difference,  $[N]^{k+1} = [N]^k + (S^k - D^k)\Delta t$ . (  $[ ]$  is used to denote concentration.) CLM replaces  $D^k$  with  $\min(D^k, [N]^k/\Delta t)$  so that  $[N]^{k+1} \geq S^k\Delta t \geq 0$ . As a result,  $[N]$  is nonnegative in CLM (Tang and Riley, 2015).

Geochemical codes generally use implicit time stepping such as the backward Euler method,  $([N]^{k+1} - [N]^k)/\Delta t = S^{k+1} - D^{k+1}$ . Solving this nonlinear equation with the Newton-Raphson method to iterate from  $p$  to  $p + 1$ , the residual  $f = ([N]^{k+1,p} - [N]^k)/\Delta t - S^{k+1,p} + D^{k+1,p}$ , the derivative  $f' = 1/\Delta t - \partial S^{k+1,p}/\partial[N]^{k+1,p} + \partial D^{k+1,p}/\partial[N]^{k+1,p}$ , the update  $\delta = f/f'$ , and  $[N]^{k+1,p+1} = [N]^{k+1,p} - \delta$ . Depending on  $[N]^k$ ,  $\Delta t$ ,  $S^{k+1,p}$ ,  $D^{k+1,p}$ , and the derivatives,  $[N]^{k+1,p+1}$  can be negative, which is not physical, and can cause numerical instability and errors (Shampine et al., 2005). With instability, the simulation may abort before reaching target simulation duration. Excess numerical error may jeopardize the improvements in process representation. Avoiding numerical instability and error may result in small time step sizes and high computational cost. Therefore, it is necessary to address the nonphysical solution negativity for accurate, robust, and efficient numerical simulation.

Enforcing nonnegativity is a common challenge in science, engineering, and business, including, for example, image processing, optimization, and ecosystem and geochemical modeling (Antonelli et al., 2009; Broekhuizen et al., 2008; Bruggeman et al., 2007; Burchard et al., 2003, 2005; Chen and Plemmons, 2009; Pierre and Schmitt, 2000; Shampine et al., 2005). The challenge increases in geochemical modeling because the concentration can be very low. For example, the threshold concentration for  $H_2$  is 1.5 nM ( $10^{-9}$  M) for dechlorinators and 5~20 nM for methanogens (Fennell and Gossett, 1998). US Environmental Protection Agency maximum contaminant level for drinking water for dioxin is 30 ppq ( $3.5 \times 10^{-13}$  M). The redox potential Eh needs to be decreased to  $-0.35$  V (corresponding to an  $O_2$  concentration  $< 10^{-22}$  M Hungate, 1975) for methanogens to grow (Jarrell, 1985). With very low concentration, a small consumption or numerical overshoot can lead to negative concentration.

Two methods are used to avoid negative concentration in geochemical codes. One is to use the logarithm concentration as the primary variable (Bethke, 2007; Hammond, 2003; Parkhurst and Appelo, 1999). Log transformation (LT) is well suited for solving the mass action equations because it converts these nonlinear equations into linear equations. However, LT converts linear advection and diffusion equations into nonlinear equations, which may increase the computational cost (Hammond, 2003). The other approach scales back the update in each of the Newton-Raphson iteration (SU) to enforce nonnegativity (Bethke, 2007; Hammond, 2003). Both methods are available in PFLOTRAN (Lichtner et al., 2015) (with SU as the default) and some other geochemical codes (e.g., Geochemist's Workbench, Bethke, 2007). However, to our knowledge, the implications of these approaches have not been thoroughly examined, particularly for application to CLM.

Competition for substrates (for instance, labile carbon, phosphate,  $O_2$ , and  $H_2$ ) is common in terrestrial ecosystems, and is increasingly incorporated in process-rich models. As the terrestrial ecosystem models are often run under a variety of conditions around the globe for hundreds of years with a time step as small as half an hour, proper treatment of the nonphysical solution negativity is necessary for accurate, efficient, and robust simulation of biogeochemical processes using reactive transport codes. The objective of this work is to implement CLM subsurface biogeochemical reac-

tions in CLM-PFLOTRAN with a focus of addressing the nonphysical solution negativity to obtain  
110 accurate, efficient, and robust solutions. We implement the CLM-CN decomposition (Bonan et al.,  
2012; Oleson et al., 2013; Thornton and Rosenbloom, 2005); nitrification; denitrification (Dickinson  
et al., 2002; Parton et al., 2001, 1996); and plant nitrogen uptake reactions in CLM-PFLOTRAN and  
test the implementation at arctic, temperate, and tropical sites. In addition to SU and LT, we examine  
ways to downregulate consumption rate to account for the limitation of reactant availability on reac-  
115 tion rate. This work focuses on addressing the nonphysical solution negativity for biogeochemistry,  
comprehensive CLM-PFLOTRAN coupling in heat transfer (including freeze and thaw), hydrology,  
and biogeochemistry will be presented in future publications. While we use CLM-PFLOTRAN to  
implement and test simple carbon and nitrogen reactions at a few sites, we hope that what we develop  
here will be applicable for a wide range of applications.

## 120 2 CLM-PFLOTRAN biogeochemistry

The terrestrial ecosystem models generally include biogeochemical reactions for carbon and nitro-  
gen cycles, in particular, the organic matter decomposition, nitrification, denitrification and methane  
production and oxidation. The kinetics are usually described by a first-order rate modified by re-  
sponse functions for environmental variables (temperature, moisture, pH, etc.) (Bonan et al., 2012;  
125 Boyer et al., 2006; Schmidt et al., 2011). In this work, we use the CLM-CN decomposition (Bo-  
nan et al., 2012; Oleson et al., 2013; Thornton and Rosenbloom, 2005), nitrification, denitrification  
(Dickinson et al., 2002; Parton et al., 2001, 1996), and plant nitrogen uptake reactions (Fig. 1) as an  
example. The reactions and rate formulae are detailed in Appendix A.

In CLM-PFLOTRAN, CLM instructs PFLOTRAN to solve the partial differential equations for  
130 energy (including freezing and thawing), water flow, and reaction and transport in the surface and  
subsurface. This work focuses on the biogeochemistry. Specifically, we focus on addressing the  
nonphysical solution negativity for the geochemical reactions, with CLM solving the energy and  
water flow equations and handling the solute transport (mixing, advection, diffusion, and leaching).

In each CLM time step, CLM provides production rates for Lit1C, Lit1N, Lit2C, Lit2N, Lit3C,  
135 Lit3N for litter fall; CWDC, and CWDN for coarse woody debris production,  $\text{NH}_4^+$  and  $\text{NO}_3^-$  for  
nitrogen deposition and fixation; and plant N demand (rate); and specifies liquid water content, ma-  
trix potential and temperature for PFLOTRAN; PFLOTRAN solves the ordinary differential equa-  
tions for the kinetic reactions, the mass action equations for the equilibrium equations, and provides  
the final concentrations back to CLM.

140 PFLOTRAN does not track individual reaction rates such as total nitrogen mineralization rate. We  
add optional hypothetical species (diagnostic variables), e.g., PlantA, PlantN,  $\text{N}_2\text{O}$ , and DeniN,  
to track  $\text{NO}_3^-$  uptake by plants as in reactions (R13,R14);  $\text{N}_2\text{O}$  production from nitrification reaction  
(R11) due to net mineralization (Eq. A5); and denitrification (R12). At the end of each time step,

CLM uses the change of these concentrations to calculate the specific rates. To simplify the calculations, we reset these concentrations to  $10^{-10}$  at the beginning of each time step instead of storing the values of the previous time step.

The reactions and rates in Appendix A are implemented using the “reaction sandbox” concept in PFLOTRAN (Lichtner et al., 2015). For each reaction, we specify a rate and a derivative of the rate with respect to any components in the rate formula, given concentrations, temperature, moisture content, grid cell volume, and other environmental variables. PFLOTRAN accumulates these rates and derivatives into a residual vector and a Jacobian matrix, and the global equation is discretized in time using the backward Euler method and solved using the Newton-Raphson method. Ignoring equilibrium reactions and transport for simplicity of discussion in this work, PFLOTRAN solves the ordinary differential equation,

$$155 \quad dc/dt = \mathbf{R}(\mathbf{c}), \quad (1)$$

with  $\mathbf{c}$  as the concentration vector and  $\mathbf{R}$  as the kinetic reaction rate. Discretizing Eq. (1) in time using the backward Euler method,

$$(c^{k+1} - c^k)/\Delta t = \mathbf{R}(c^{k+1}). \quad (2)$$

Solving the equation using the Newton-Raphson method, we denote the residual as

$$160 \quad \mathbf{f}(\mathbf{c}^{k+1,p}) = (c^{k+1,p} - c^k)/\Delta t - \mathbf{R}(c^{k+1,p}), \quad (3)$$

and Jacobian as

$$\mathbf{J} = \frac{\partial \mathbf{f}(\mathbf{c}^{k+1,p})}{\partial \mathbf{c}^{k+1,p}}, \quad (4)$$

the update is

$$\delta \mathbf{c}^{k+1,p} = \mathbf{J}^{-1} \mathbf{f}(\mathbf{c}^{k+1,p}), \quad (5)$$

165 and the iteration equation is

$$\mathbf{c}^{k+1,p+1} = \mathbf{c}^{k+1,p} - \delta \mathbf{c}^{k+1,p}. \quad (6)$$

The iteration continues until either the residual  $\mathbf{f}(\mathbf{c}^{k+1,p})$  or the update  $\delta \mathbf{c}^{k+1,p}$  is less than a specified tolerance. Specifically,

$$\|\mathbf{f}(\mathbf{c}^{k+1,p})\|_2 < \text{ATOL}, \quad (7)$$

170

$$\begin{aligned} \|\mathbf{f}(\mathbf{c}^{k+1,p})\|_2 &< \text{RTOL}, \\ \|\mathbf{f}(\mathbf{c}^{k+1,0})\|_2 & \end{aligned} \quad (8)$$

or

$$\frac{\|\delta\mathbf{c}^{k+1,p}\|_2}{\|\mathbf{c}^{k+1,p}\|_2} < \text{STOL}. \quad (9)$$

If none of these tolerances are met in MAXIT iterations or MAXF function evaluations, the iteration is considered to diverge, and PFLOTRAN decreases the time step size for MAX\_CUT times. The default values in PFLOTRAN are ATOL =  $10^{-50}$ , RTOL =  $10^{-8}$ , STOL =  $10^{-8}$ , MAXIT = 50, MAXF =  $10^4$ , and MAX\_CUT = 16.

Unlike the explicit time stepping in CLM for biogeochemistry where only the reaction rates need to be calculated, the implicit time stepping requires the derivatives. While PFLOTRAN provides the option to calculate the derivatives numerically, analytical derivative calculation is generally preferred (e.g., Xu et al., 2006) because numerical calculation for accurate Jacobian approximation is a notoriously difficult task (Shampine et al., 2005).

Many reactions can be specified, and the rates and derivatives are accumulated in the residual and Jacobian, providing flexibility in specifying various reactions with a user-defined rate formula. As typical rate formulae consist of first order, Monod, and/or inhibition terms, a general rate formula with flexible number of terms and typical moisture, temperature, and pH response functions are coded in PFLOTRAN. Most of the biogeochemical reactions can be specified in the input file, with flexible number of reactions, pools (species), rate terms, and various response functions without source code modification. Code modification is necessary only when different rate formulae, or response functions are introduced. In contrast, the number of pools and reactions are traditionally hard-coded in CLM. Consequently, any change of the pools, reactions, or rate formula may require source code modification. Therefore, this new approach facilitates implementation of increasingly mechanistic reactions and tests of various representations with less code modifications.

### 3 Approaches for addressing the nonphysical solution negativity

One of the basic challenges for using a numerical geochemical formulation for CLM is that the updated solution in Eq. (6) is not guaranteed to be nonnegative. Both SU (scaling back the update during each iteration) and LT (log transformation) are available in PFLOTRAN to enforce nonnegativity. However, to our knowledge, the limitations and implications of both methods have not been thoroughly examined.

#### 3.1 Scaling back update in iterations

SU scales back the update (Eq. 6) with a scaling factor  $\lambda$  (Bethke, 2007; Hammond, 2003) such that

$$\mathbf{c}^{k+1,p+1} = \mathbf{c}^{k+1,p} - \lambda \delta\mathbf{c}^{k+1,p} > 0, \quad (10)$$

where

$$205 \quad \lambda = \alpha \min [1, \mathbf{c}^{k+1,p}(i)/\delta\mathbf{c}^{k+1,p}(i)] \quad (11)$$

for positive  $\delta\mathbf{c}^{k+1,p}(i)$  and  $i = 1$  to  $m$ , with  $m$  as the number of species times the number of numerical grid cells. With SU, the concentration of the species that is going negative decreases by  $(1 - \alpha)$  times in each iteration instead. This can be shown by solving the zero-order uptake problem  $dc/dt = -1$ :  $c^{k+1} = c^k - \Delta t$  when  $\Delta t \geq c^k$ ; otherwise,  $\lambda = \alpha c^k / \Delta t$ , and  $c^{k+1} = (1 - \alpha)c^k$ .

210 With a default  $\alpha = 0.99$  in PFLOTRAN, each iteration decreases the concentration by 100 times. With multiple iterations, the concentration can approach machine precision or zero (we use zero for concentration below machine precision in this work).

If  $\mathbf{c}^{k+1,p}(i)$  is 0, and  $\delta\mathbf{c}^{k+1,p}(i) > 0$ , then  $\lambda = 0$ , and the update is limited to 0. Even if  $\lambda = 0$  occurs in only one grid cell for only one species, the update for all of the species and all of the grid 215 cells are constrained to 0, and the residual will not be decreased to satisfy Eqs. (7 or 8) to achieve convergence. If the iteration is deemed converged because the scaled update is 0, and Eq. (9) is met, the calculation will march through this time step without any change in the concentrations, numerically stopping all reactions. This can continue for many time steps until  $\delta\mathbf{c}^{k+1,p}(i)$  becomes negative.

220 Application of a very small scaling factor  $\lambda$  due to decrease of a small concentration for one species may have a similar consequence: the iteration may not decrease the residual  $\mathbf{f}(\mathbf{c}^{k+1,p})$  or the iteration may not converge because Eqs. (7 or 8) are not met. If the iteration is considered converged because of too small an update  $\lambda\delta\mathbf{c}^{k+1,p}$  (Eq. 9 is satisfied), the scaling factor  $\lambda$  (e.g.,  $10^{-10}$ ) may correctly limit the consumption reaction rates to account for availability limitation, but wrongly 225 limit the production rate in the time step. This can be illustrated by adding to the zero-order uptake problem  $dc/dt = -1$  an independent zero order production  $de/dt = 1$ : when  $\Delta t \geq c^k$ ,  $\lambda = \alpha c^k / \Delta t$ ,  $c^{k+1} = (1 - \alpha)c^k$ ,  $e^{k+1} = e^k + \alpha c^k$  rather than  $e^{k+1} = e^k + \Delta t$ . If  $c^k = 0$ , SU numerically stops the independent production reaction. To avoid excessive numerical error, PFLOTRAN reports an error and exits when  $\lambda < \lambda_{\min}$ , with default  $\lambda_{\min} = 10^{-10}$ , translating the accuracy issue into a stability 230 issue. It is necessary to investigate SU to resolve accuracy and stability issues.

### 3.2 Log transformation

LT is widely used in geochemical codes for describing highly variable concentrations for primary species such as  $H^+$  or  $O_2$  that can vary over many orders of magnitude as pH or redox state changes without the need to use variable switching. It is also used to enforce positivity (Bethke, 2007; Hammond, 2003; Parkhurst and Appelo, 1999). Instead of solving Eq. (3) for  $\mathbf{c}^{k+1}$  using Eqs. (4,5,6), LT solves for  $(\ln \mathbf{c}^{k+1})$  with

$$\mathbf{J}_{\ln}(i,j) = \frac{\partial \mathbf{f}(i)}{\partial \ln(\mathbf{c}(j))} = \mathbf{c}(j) \frac{\partial \mathbf{f}(i)}{\partial \mathbf{c}(j)} = \mathbf{c}(j) \mathbf{J}(i,j), \quad (12)$$

$$\delta \ln \mathbf{c}^{k+1,p} = \mathbf{J}_{\ln}^{-1} \mathbf{f}(\mathbf{c}^{k+1,p}), \quad (13)$$

240 and

$$\mathbf{c}^{k+1,p+1} = \mathbf{c}^{k+1,p} \exp[-\delta \ln(\mathbf{c}^{k+1,p})]. \quad (14)$$

One downside is apparent from Eq. (12): suppose  $\mathbf{c}^{k+1,p}(j)$  is  $10^{-10}$ ;  $\mathbf{J}(i,j)$  (column  $j$  of the Jacobian) decreases by  $10^{10}$  times to  $\mathbf{J}_{\ln}(i,j)$ . As a result, the condition number of the Jacobian matrix may increase by orders of magnitude, which may constrain the time step size to be substantially reduced, compared to the case without LT. Secondly, the small eigenvalues may result in large  $\delta \ln \mathbf{c}^{k+1,p}$ , which may cause overshooting to an unrealistically large concentration (negative update), or essentially 0 concentration (positive update), or even overflow in the exponential function in Eq. (14). To prevent these problems, PFLOTRAN limits the update to

$$\delta \ln(\mathbf{c}^{k+1,p}) = \text{sign}[\delta \ln(\mathbf{c}^{k+1,p})] \min[\text{abs}(\delta \ln \mathbf{c}^{k+1,p}), \delta_{\ln,\max}] \quad (15)$$

250 with a default  $\delta_{\ln,\max} = 5$ . Thirdly, LT does not prevent zero concentration per se: a number of iterations with positive  $\delta \ln \mathbf{c}^{k+1,p}(j)$  update can bring  $\mathbf{c}^{k+1,p+1}(j)$  to zero. With zero concentration,  $\mathbf{J}_{\ln}$  becomes singular, and the numerical solution fails. These can be shown by solving  $dc/dt = -1$  in the log transformed form  $d \ln c/dt = -1/c$ :  $c^{k+1} = c^k e^{-\Delta t/c^{k+1}}$ . LT converts the linear problem that does not require iteration to a nonlinear problem that needs to be solved iteratively. As  $c^{k+1}$  255 becomes small,  $\Delta t$  has to be decreased accordingly, or the concentration goes to zero and causes division by 0 overflow.

### 3.3 Downregulation of reaction rate

Even though ensuring nonnegativity, neither SU nor LT can prevent zero concentrations, which can cause numerical problems for both. They require the solution to the mathematical representation 260 itself be positive. To obtain such a representation, it is necessary to downregulate reaction rates to represent the limitation of the availability of each reactant on the reaction rate. In the geochemical modeling literature, this is mostly represented by a rate limiting function as a function of concentration in each reaction for each reactant. CLM downregulates demand (consumption) as a function of rate (demand-based competition) (Tang and Riley, 2015). We further examine downregulation of 265 consumption rate as a function of concentration (DC) and rate (DR) for use with SU or LT to address the nonphysical solution negativity.

#### 3.3.1 Downregulation of consumption rate as a function of concentration

The first-order decay problem (Eqs. A1, A4, A7, A9) is nonnegative. This can be shown by solving the first-order problem  $dc/dt = -c$  using either the analytical solution  $c^{k+1} = c^k e^{-\Delta t}$  or the backward Euler method  $c^{k+1} = c^k / (1 + \Delta t)$ ; However, it can go to zero. To avoid zero concentration,

a residual term is often used to limit the decay to a residual concentration (Tang et al., 2013a). For example, Eq. (A1) becomes

$$\frac{d[\text{CN}_u]}{dt} = -k_d f_T f_w ([\text{CN}_u] - [\text{CN}_u]_r). \quad (16)$$

When the concentration goes below  $[\text{CN}_u]_r$  in an iteration, Eq. (16) implies a hypothetical reverse reaction to bring it back to  $[\text{CN}_u]_r$ . An alternative is to use a cutoff (Appendix B). Even though it can be smoothed, a cutoff is still a sharp change as shown in the derivative (Fig. 14). In contrast, the residual concentration introduced in Eq. (16) does not change the derivative.

For the litter decomposition reactions (R7, R8, R9) that immobilize nitrogen, and nitrification reaction (R11) associated with decomposition to produce  $\text{N}_2\text{O}$ , the rate formulae (e.g., Eq. A1, 16,) do not account for the limitation of the reaction rate by the availability of nitrogen. They are zero order with respect to nitrogen. Mechanistically, a nitrogen-limiting function needs to be added to those formulae to represent the limitation of decreasing nitrogen concentration on decomposition rate (downregulation), for example,

$$\frac{d[\text{CN}_u]}{dt} = -k_d f_T f_w ([\text{CN}_u] - [\text{CN}_u]_r) f([N]). \quad (17)$$

A widely used downregulation function is the Monod substrate limitation function (Hammond, 2003; Tang et al., 2013a):

$$f([N]) = \frac{[N]}{[N] + k_m}, \quad (18)$$

with half saturation  $k_m$ . In the case of  $[N] = k_m$ ,  $f([N]) = 0.5$ . For  $[N] \gg k_m$ , Eq. (18) is zero order with respect to  $[N]$  or has little impact on the decomposition reactions that immobilize N. For  $[N] \ll k_m$ , Eq. (18) approximates first order with respect to  $[N]$  (Figure 15d). Nevertheless, since  $\frac{df([N])}{d[N]} = \frac{k_N}{([N]+k_m)^2}$ , the derivative increases to about  $k_m^{-1}$  as the concentration decreases to below  $k_m$  (Fig. 15). This is similar to the smoothed cutoff in Eq. (B2) (Fig. 14): even though smoothed, it is still a steep transition.

To represent the threshold concentration beyond which certain microorganisms can not use certain electron donors (Fennell and Gossett, 1998), and prevent zero concentration, a residual concentration can be added to Eq. (18) as  $f([N]) = \frac{[N] - [N]_r}{[N] - [N]_r + k_m}$ . Similar to Eq. (16), this implies a nonphysical backward reaction when  $[N] < [N]_r$ . If we use the cutoff instead of a residual concentration, a combination of Eqs. (18) and (B2) produces more nonlinearity, as evidenced in Fig. (16), which may result in small time step sizes to march through these transition regions when the concentration gets there.

The plant nitrogen uptake reactions (R13, R14) are zero order, and substrate limiting functions need to be added as well. For plant uptake and immobilization, we have to distribute the demands between  $\text{NH}_4^+$  and  $\text{NO}_3^-$ . If we simulate the  $\text{NH}_4^+$  limitation on plant uptake, e.g., with

$$R_a = R_p \frac{[\text{NH}_4^+]}{[\text{NH}_4^+] + k_m}, \quad (19)$$

the  $\text{NO}_3^-$  plant uptake can be represented by

$$305 \quad R_n = (R_p - R_a) \frac{[\text{NO}_3^-]}{[\text{NO}_3^-] + k_m} = R_p \frac{k_m}{[\text{NH}_4^+] + k_m} \frac{[\text{NO}_3^-]}{[\text{NO}_3^-] + k_m}. \quad (20)$$

This essentially assumes an inhibition of  $\text{NH}_4^+$  on  $\text{NO}_3^-$  uptake, which is consistent with the observation that plant  $\text{NO}_3^-$  uptake rate remained low until  $\text{NH}_4^+$  concentrations dropped below a threshold (Eltrop and Marschner, 1996).

For comparison with CLM, we examine the uptake rate as a function of demands and available concentrations  $f_{pi} = R_a + R_n/R_p$ . As an example, we consider uptake  $R_p = 10^{-9} \text{ M s}^{-1}$  from a solution with various  $[\text{NH}_4^+]$  and  $[\text{NO}_3^-]$  for a 0.5 h time step. With CLM,  $f_{pi} = 1$  when  $[\text{NH}_4^+] + [\text{NO}_3^-] \geq R_p\Delta t$ ; otherwise, it decreases with decreasing  $[\text{NH}_4^+] + [\text{NO}_3^-]$  (Fig. 2). The new representation (Eqs. 19, 20) is generally similar, with  $f_{pi} = 1$  or 0 when  $[\text{NH}_4^+]$  or  $[\text{NO}_3^-] \gg$  or  $\ll k_m$ . For the intermediate concentrations,  $f_{pi}$  in the new scheme is less than or equal to that in CLM because  $\text{NH}_4^+$  “inhibits”  $\text{NO}_3^-$  uptake. The difference decreases with decreasing  $k_m$ , apparently disappearing at  $k_m = 10^{-10}$  (Fig. 3).

Various level of preferences of  $\text{NH}_4^+$  over  $\text{NO}_3^-$  uptake were observed for plants (Pfautsch et al., 2009; Warren and Adams, 2007; Nordin et al., 2001; Falkengren-Grerup, 1995; Gherardi et al., 2013). The microbial uptake of inorganic and organic nitrogen species is similar (Fouilland et al., 2007; Kirchman, 1994; Kirchman and Wheeler, 1998; Middelburg and Nieuwenhuize, 2000; Veugel et al., 2004). CLM implies a strong preference for  $\text{NH}_4^+$  over  $\text{NO}_3^-$ . For example, if  $\text{NH}_4^+$  is abundant,  $\text{NO}_3^-$  will not be taken. The new scheme allows the level of preference to be adjusted by varying  $k_m$ .

### 3.3.2 Downregulation of consumption as a function of rate

325 DC involves adding residual concentration and half saturations, which has the potential to provide mechanistic treatment of the processes. It also introduces a number of parameters that need to be determined. These parameters may not be well defined and can vary among different microbe and plant species under various conditions across the globe. An alternative is to downregulate consumption as a function of rate (DR) like CLM demand-based competition.

330 CLM splits the available nitrogen to meet the demands by microbes and plants in proportion to the potential rates (Thornton and Rosenbloom, 2005; Oleson et al., 2013) (Appendix A5). Suppose that the demand (consumption, sink, including immobilization, plant uptake, nitrification, etc.) rate is  $R_{dp}$ ; the supply (source, production, including deposition, mineralization, etc.) rate is  $R_s$ , and the concentration is  $[N]$  at the beginning of the time step, the demand is downregulated to

$$335 \quad R_d = \min [R_{dp}, R_s + [N]/\Delta t]. \quad (21)$$

Tang and Riley (2015) suggest to include  $R_s$ . For a reaction that is limited by multiple substrates (e.g., nitrogen and phosphorus), they use the minimum of the downregulated rates. Like the demand

based competition in CLM, this is simple to implement, and prevents negative concentration when the explicit forward difference method is used. It is different for the backward Euler method. Applying to  $dc/dt = -1$ ,  $c^{k+1} = c^k - \Delta t$  for  $c^k \geq \Delta t$ ; for  $c^k < \Delta t$ ,  $c^{k+1} = c^k/2$ : the concentration decreases by half in a time step. This is similar to SU with  $\alpha = 0.5$ , which is suggested by Bethke (2007). DR essentially downregulates the demands using the first-order rate when nitrogen is limiting. Eq. (21) is similar to Eq. (18), except that Eq. (18) switches from zero to the first-order rate smoothly, while Eq. (21) has a discontinuity.

Implementation of DR in a geochemical code like PFLOTRAN involves separating the supply and consumption rates for each species in each reaction, and checking and conducting downregulation when necessary after contributions from all of the reactions are accumulated. It involves not only the rate terms for the residual but also the derivative terms for the Jacobian. The complexity explodes when more species needs to be downregulated (e.g.,  $\text{NH}_4^+$ ,  $\text{NO}_3^-$ , and organic N) and there are transformation processes among these species. This is shown in Appendix C, which describes the implementation of downregulation of  $\text{NH}_4^+$  and  $\text{NO}_3^-$  with a nitrification reaction from  $\text{NH}_4^+$  to  $\text{NO}_3^-$ . Basically, it becomes challenging to separate, track, and downregulate consumption and production rates for an indefinite number of species, and calculation of the Jacobian becomes convoluted. This work diffs from Tang and Riley (2015) in that we use implicit time stepping while they use explicit time stepping.

#### 4 Test problems, results, and discussions

We examine the causes of negative concentration; the advantages and disadvantages of SU, LT, DC, and DR; and the accuracy, stability, and efficiency issue using both simple test problems and coupled CLM-PFLOTRAN site simulations. For simple test problems, we assess the conditions under which large updates occur. With coupled CLM-PFLOTRAN spin-up simulations for arctic, temperate, and tropical sites, we assess the conditions when the nonphysical solution negativity arises by relaxing the downregulation on nitrogen consumption (decreasing half saturation). Spreadsheet and PFLOTRAN input files are provided as supplemental information (SI).

Our implementation of CLM biogeochemistry introduces mainly two parameters: half saturation  $k_m$  and residual concentration. A wide range of  $k_m$  values were reported for  $\text{NH}_4^+$ ,  $\text{NO}_3^-$ , and organic nitrogen for microbes and plants. The median, mean, and standard deviations range from  $10 \sim 100$ ,  $50 \sim 500$ , and  $10 \sim 200 \mu\text{M}$ , respectively (Kuzyakov and Xu, 2013). Reported residual (threshold) concentrations are limited and are considered to be 0 (e.g., HØGh-Jensen et al., 1997), likely because of the detection limits of the analytical methods. The detection limits are usually at the  $\mu\text{M}$  level, while up to the nM level was reported (Nollet and De Gelder, 2013). In Ecosys, the  $k_m$  is 0.40 and  $0.35 \text{ gN m}^{-3}$ , and the residual concentration is  $0.0125$  and  $0.03 \text{ gN m}^{-3}$  (Grant, 2013) for  $\text{NH}_4^+$  and  $\text{NO}_3^-$  for microbes. We start with  $k_m = 10^{-6} \text{ M}$  or  $\text{mol m}^{-3}$ , and residual concentration  $10^{-15} \text{ M}$  or

mol m<sup>-3</sup> for plants and microbes. To further investigate the nonphysical solution negativity for the current study and for future application for other nutrients (e.g., H<sub>2</sub> and O<sub>2</sub>) where the concentrations  
375 can be much lower, we examine  $k_m$  from 10<sup>-3</sup> to 10<sup>-12</sup> in our test problems. The  $k_m$  is expected to be different for different plants, microbes, and for NH<sub>4</sub><sup>+</sup> and NO<sub>3</sub><sup>-</sup>, and different values can be assigned in the input file in our implementation. we do not differentiate them in this work as we focus on numerical issues.

#### 4.1 Plant nitrogen uptake, nitrification, and denitrification

380 It was observed that plants can decrease nitrogen concentration to below detection limits in hours (Kamer et al., 2001). Plant nitrogen uptake is one of the major sinks for nitrogen in TEMs and contributes to decreasing nitrogen concentration numerically to 0 or negative. In CLM, the total plant nitrogen demand is calculated based on photosynthesized carbon allocated for new growth and the C:N stoichiometry for new growth allocation, and the plant nitrogen demand from the soil  
385 is equal to the total nitrogen demand minus retranslocated nitrogen stored in the plants (Oleson et al., 2013). The CLM calculated rate is provided as an input to PFLOTRAN, which is constant in a 0.5 h time step. Without downregulating plant nitrogen uptake rate, nitrogen concentration is likely to go negative when the net consumption rate overwhelms a low available concentration. As the Monod substrate limiting function is the most widely used downregulation function, we  
390 examine the numerical solutions, beginning with the numerical issues during the iteration processes. Incrementally, we add first order reactions (e.g., nitrification, denitrification, and plant NO<sub>3</sub><sup>-</sup> uptake) to look into these issues in increasingly complex systems.

##### 4.1.1 Plant NH<sub>4</sub><sup>+</sup> uptake (Test 1)

We consider the plant NH<sub>4</sub><sup>+</sup> uptake reaction (R13) with the rate  $R_a$

395 
$$\frac{d[\text{NH}_4^+]}{dt} = -R_a \frac{[\text{NH}_4^+]}{[\text{NH}_4^+] + k_m} = -R_{at}. \quad (22)$$

A semi-analytical solution (Eq. D2) has one positive and one negative roots. With the positive root,  $[\text{NH}_4^+]^{k+1} \rightarrow 0$  when  $[\text{NH}_4^+]^k \rightarrow 0$ , or  $R_a \Delta t \rightarrow \infty$ . As  $k_m \rightarrow 0$ ,  $[\text{NH}_4^+]^{k+1} \rightarrow 0$  when  $[\text{NH}_4^+]^k \leq R_a \Delta t$ . If we replace  $[\text{NH}_4^+]$  with  $[\text{NH}_4^+] - [\text{NH}_4^+]_r$  in Eqs. (22) and (D2),  $[\text{NH}_4^+]^{k+1} \rightarrow [\text{NH}_4^+]_r$ . The representation of plant NH<sub>4</sub><sup>+</sup> uptake by Eq. (22) ensures  $[\text{NH}_4^+]^{k+1} \geq [\text{NH}_4^+]_r$ .

400 Solving Eq. (22) using the backward Euler method and Newton-Raphson method from time step  $k$  to  $k + 1$ , and  $[\text{NH}_4^+]^{k+1,0} = [\text{NH}_4^+]^k$ , the update for the first iteration is

$$\xi = \frac{\delta[\text{NH}_4^+]^{k+1,1}}{[\text{NH}_4^+]^{k+1,0}} = \frac{\frac{1}{[\text{NH}_4^+]^k + k_m}}{\frac{1}{R_a \Delta t} + \frac{k_m}{([\text{NH}_4^+]^k + k_m)^2}}. \quad (23)$$

The update is a function of uptake rate ( $R_a$ ), time step size ( $\Delta t$ ), concentration ( $[\text{NH}_4^+]^k$ ), and half saturation ( $k_m$ ). For  $R_a \Delta t$  from 0 to  $\infty$ ,  $\xi$  increases from 0 to  $1 + [\text{NH}_4^+]/k_m$ . With  $[\text{NH}_4^+]^k =$

405  $10^{-6}$  M, and  $k_m = 10^{-6}$  M, the update is less than  $[\text{NH}_4^+]^k$  when  $R_a\Delta t \leq 5 \times 10^{-6}$  M (say using CLM  $\Delta t = 1800$  s,  $R_a \leq 2.8 \times 10^{-9}$  mol s $^{-1}$ , Fig. 4); when  $R_a\Delta t$  increases, the update increases, with an upper limit of 2, suggesting that large time step size and uptake rate alone usually do not lead to an excessively large update or a small scaling factor. For  $[\text{NH}_4^+]^k$  from 0 to  $\infty$ ,  $\xi$  starts from  $R_a\Delta t/(k_m + R_a\Delta t)$ , increases to peak at  $\sqrt{R_a\Delta t/k_m}/2$  when  $[\text{NH}_4^+] = \sqrt{k_m R_a \Delta t} - k_m$ , and 410 then decreases to 0. With  $k_m = 10^{-6}$  M and  $R_a\Delta t = 0.001$  M,  $\xi$  starts from  $\sim 1$ , increases to peak at  $\sim 16$  when  $[\text{NH}_4^+]^k = 3 \times 10^{-5}$ , and decreases to 0 as  $[\text{NH}_4^+]^k \rightarrow \infty$ . For  $k_m$  from  $\infty$  to 0,  $\xi$  increases from 0 to  $R_a\Delta t/k_m$ . With  $R_a\Delta t = 10^{-3}$ , and  $[\text{NH}_4^+]^k = 10^{-6}$ , the update increases several orders of magnitude as  $k_m$  decreases from  $10^{-6}$  to  $10^{-9}$ , with a limit of  $\xi = 10^3$  (Fig.4). While the semi-analytical solution (Eq. D2) indicates that the problem itself is nonnegative, these 415 calculations suggests that overshoot can occur, and large time step, uptake rate, low concentration and half saturation can contribute to large update that can exceed the available concentration by orders of magnitude.

Now we look into the iteration processes: the solution starts with an overshoot to  $1.995 \times 10^{-6}$  and converges to the positive semi-analytical solution  $3.1127 \times 10^{-5}$  (Eq. D2) in eight iterations 420 when  $R_a\Delta t = 0.001$  (SI spreadsheet).  $dR/dC$  changes from  $\sim 1$  to  $10^5$  in the first iteration, although the change in the Jacobian is reduced due to a small  $R_a\Delta t$ . With  $R_a\Delta t = 0.002$ , the update  $\delta$  is greater than  $[\text{NH}_4^+]_k$ ; without scaling back the update, the solution converges to the negative solution  $-1.002 \times 10^{-3}$  (SI, negative root from Eq. D2). Scaling back the update with  $\alpha = 0.9999$ , the concentration decreases by  $1 - \alpha = 10^{-4}$  times in the first iteration rather than to negative root (SI). 425 The solution converges to the positive root in seven iterations.

If LT is used with  $R_a\Delta t = 0.002$ , the solution oscillates and results in a  $\delta$  of  $-1041.5$  in the fifth iteration, which essentially makes the solution 0 (SI). Limiting  $\delta \leq \delta_{\ln,\max}$ , the solution converges to the semi-analytical solution (Eq.D2) in 7, 7, 6, 5, 6, and 8 iterations with  $\delta_{\ln,\max} = 2, 3, 4, 5, 6$ , and 7, respectively. For  $\delta_{\ln,\max} \geq 8$ , the iteration oscillates and converges slowly. If we split  $R_a\Delta t$  430 = 0.002 into two steps, the first step takes seven iterations to converge, while the second step takes nine iterations, with  $\delta_{\ln,\max} = 5$ .

Finally, we consider a PFLOTRAN simulation: a  $1 \text{ m} \times 1 \text{ m} \times 1 \text{ m}$  grid cell, with 0.25 water content, initial  $4 \mu\text{M}$   $\text{NH}_4^+$ , and a plant  $\text{NH}_4^+$  demand  $10^{-7}$  mol s $^{-1}$  ( $\sim 3 \text{ mg d}^{-1}$ , reported values for evergreen and deciduous forest range from  $0.3 \sim 10 \text{ g m}^{-2}$  year, Chapin et al., 2011). It takes 435 10,000 s (2.78 h) to consume  $\text{NH}_4^+$ . We use a time step of 0.5 h for a simulation duration of 10 h. Without downregulating the uptake rate, SU decreases  $[\text{NH}_4^+]$  to 0 and then keeps it 0 as  $\lambda = 0$ . With LT, we obtain an accurate solution until it fails when the concentration goes to 0, and the Jacobian becomes singular.

Using SU with DC with a residual concentration  $[\text{NH}_4^+]_r$  of  $10^{-20}$  M and a half saturation  $k_m$  440 of  $10^{-6}$ ,  $10^{-9}$ , or  $10^{-12}$ , the calculated concentration  $[\text{NH}_4^+]$  is kept to be greater than or equal to  $10^{-20}$  (Fig. 5). With a  $k_m$  of  $10^{-6}$ , the calculated  $[\text{NH}_4^+]$  is above  $10^{-20}$ , and the update does not

exceed the concentration in any iteration during the 10 h simulation duration. With a  $k_m$  of  $10^{-9}$  and  $10^{-12}$ , the update exceeds the concentration from time 2.5 h to 3.0 h. In the case of  $k_m = 10^{-12} \text{ M}$  for the next time step, the two iterations decrease the concentration by 10,000 times, and the solution is deemed converged as the default STOL =  $10^{-8}$  is met. This continues for another time step with one iteration (Fig. 5). In these two time steps, the solution does not converge to the exact solution. If we set the residual concentration to  $10^{-15}$ , the false convergence results in a concentration below  $10^{-15}$  ( $8.71 \times 10^{-16}$ ) in the first of the two time steps. If we set STOL =  $10^{-50}$  to avoid the convergence due to Eq. (9), PFLOTTRAN cuts the time step sizes and quits due to too many cuts.

Using LT can avoid the false convergences in this example, but it requires more iterations, with 56/95, 36/110, and 32/87 for SU/LT for  $k_m$  values of  $10^{-6}$ ,  $10^{-9}$ , and  $10^{-12} \text{ M}$ , respectively. These results demonstrate that SU ensures nonnegativity and allows large time step for efficiency at the risk of inaccuracy. LT is accurate but requires more iterations.

#### 4.1.2 Plant $\text{NH}_4^+$ uptake and nitrification (Test 2)

Adding a nitrification reaction (R10) with a first-order rate, Eq. (22) becomes

$$\frac{d[\text{NH}_4^+]}{dt} = -R_a \frac{[\text{NH}_4^+]}{[\text{NH}_4^+] + k_m} - k_{nitr} [\text{NH}_4^+] = -R_{at} - R_{nitr}. \quad (24)$$

With  $J_{at} = \frac{dR_{at}}{d[\text{NH}_4^+]} = R_a \frac{k_m}{([\text{NH}_4^+] + k_m)^2}$ , and  $J_{nitr} = \frac{dR_{nitr}}{d[\text{NH}_4^+]} = k_{nitr}$  and using the backward Euler method and Newton-Raphson method, Eq. (5) becomes Eq. (E1). For plant ammonium uptake,

$$\delta[\text{PlantA}]^{k+1,1} = J_{at} \delta[\text{NH}_4^+]^{k+1,1} - R_{at} = -\frac{\frac{1}{\Delta t} + J_{nitr}}{\frac{1}{\Delta t} + J_{at} + J_{nitr}} R_{at} + \frac{J_{at}}{\frac{1}{\Delta t} + J_{at} + J_{nitr}} R_{nitr}, \quad (25)$$

A positive component,  $\frac{J_{at}}{\frac{1}{\Delta t} + J_{at} + J_{nitr}} R_{nitr}$ , is introduced even though there is no reaction that consumes PlantA. Depending on the relative magnitude of the rates ( $R_{at}$  and  $R_{nitr}$ ) and the derivatives ( $J_{at}$  and  $J_{nitr}$ ), as well as time step size  $\Delta t$  and  $[\text{NH}_4^+]^k$ , the update can be positive, which can result in too small a scaling factor that causes a nonphysical solution negativity if [PlantA] is very small. This demonstrates that products as well as reactants can be driven negative during the Newton-Raphson iterations.

This can also be shown with a simple first-order reaction  $A \rightarrow B$  with rate  $k[A]$ : taking out the equation for B,  $-k\delta[A] + \delta[B]/\Delta t = -k[A]$ ,  $\delta[B] = k\Delta t(\delta[A] - [A])$ . Suppose  $\delta[A] = 2 \times 10^{-6}$ ,  $[A] = 10^{-6}$ , and  $k\Delta t = 10^{-3}$ , then  $\delta[B] = 10^{-9}$ . If [B] is very small, say  $10^{-20}$ , this results in a  $\lambda = 0.99 \times 10^{-11}$ . This has an implication for DR: downregulating only some reactants may not be sufficient to guarantee positivity, while downregulating both reactants and products is complicated.

#### 4.1.3 Plant uptake, nitrification, and denitrification (Test 3)

Adding plant  $\text{NO}_3^-$  uptake reaction (R14) with rate  $R_{nt} = R_p \frac{[\text{NH}_4^+]}{[\text{NH}_4^+] + k_m} \frac{[\text{NO}_3^-]}{[\text{NO}_3^-] + k_m}$ ,  $J_{nt,n} = \frac{dR_{nt}}{d[\text{NO}_3^-]} = R_p \frac{[\text{NH}_4^+]}{[\text{NH}_4^+] + k_m} \frac{k_m}{([\text{NO}_3^-] + k_m)^2}$ , and  $J_{nt,a} = \frac{dR_{nt}}{d[\text{NH}_4^+]} = \frac{dR_n}{d[\text{NH}_4^+]} \frac{k_m}{([\text{NH}_4^+] + k_m)^2} \frac{[\text{NO}_3^-]}{[\text{NO}_3^-] + k_m}$ , and denitrification

reaction (R12) with rate  $R_{deni} = k_{deni}[\text{NO}_3^-]$ , and  $J_{deni} = \frac{dR_{deni}}{d[\text{NO}_3^-]} = k_{deni}$ , Eq. (5) becomes Eq. 475 (F1). For  $\text{NO}_3^-$ ,

$$\delta[\text{NO}_3^-]^{k+1,1} \left( \frac{1}{\Delta t} + J_{nt} + J_{deni} \right) = (J_{nitr} - J_{nt,a})(R_{at} + R_{nitr}) \delta[\text{NH}_4^+]^{k+1,1} - R_{nitr} + R_{nt} + R_{deni}. \quad (26)$$

In addition to plant  $\text{NH}_4^+$  uptake and nitrification,  $\delta[\text{NO}_3^-]^{k+1,1}$  becomes a function of plant  $\text{NO}_3^-$  uptake and denitrification, and all of the rate coefficients and derivatives may contribute to a positive update that can result in too small a scaling factor. Even though the problem itself is nonnegative, 480 coupling these reactions together in the Newton-Raphson iteration does introduce the potential to produce relatively significant positive update for  $\text{NO}_3^-$  and PlantN. It worsens when the interdependent uptake of  $\text{NH}_4^+$  and  $\text{NO}_3^-$  (Eqs. 19 and 20) representation brings in the impact of any rates related to  $\text{NH}_4^+$  (including deposition, uptake, immobilization, etc.), with potentially large derivative terms for the off-diagonal entries in the Jacobian matrix. It is the nonlinearity introduced in the 485 downregulation and propagated through the reactions that causes the challenge. A smaller half saturation introduces a greater derivative change; therefore, it is more likely to cause the problem. These results also suggest that the likelihood for  $\text{NO}_3^-$  to go negative is greater than  $\text{NH}_4^+$ , and PlantN is greater than PlantA as the latter are influenced by more rates and derivatives.

#### 4.2 N immobilization, mineralization, and nitrification during decomposition (Test 4)

490 We further examine the implications of a small half saturation on the numerical solutions with a decomposition test problem. We consider a case of decomposing 0.2 M Lit1C + 0.005 M Lit1N to produce SOM1 with an initial 4  $\mu\text{M}$   $\text{NH}_4^+$  using the reactions (R7 and R2) in the CLM-CN reaction network (Fig. 1) at first. Then we add the nitrification reaction (R11) with rate (Eq. A5) to examine the implications of a complex rate formula. We use PFLOTRAN with a fully saturated grid cell of 1 495 m and porosity of 0.25.

Lit1 decomposes fast at the beginning and then slows down as  $\text{NH}_4^+$  is depleted (Fig. 6). The Lit1 decomposition rate is controlled by the mineralization rate from SOM1 decomposition. As the immobilization rate decreases with decreasing Lit1,  $[\text{NH}_4^+]$  rebounds. For  $k_m$  of  $10^{-6}$ ,  $10^{-9}$ , and  $10^{-12}$  M, Lit1 and SOM1 dynamics are similar, but the  $[\text{NH}_4^+]$  values are decreased to  $\sim 10^{-8}$ , 500  $10^{-11}$ , and  $10^{-14}$  M, respectively. The number of iterations for SU/LT is 76/169, 68/194, and 54/207 for the three  $k_m$  values. Obviously, smaller  $k_m$  results in lower  $[\text{NH}_4^+]$  and more iterations.

The implication of  $k_m = 10^{-12}$  becomes obvious when the nitrification reaction (R11) with rate (Eq. A5 with downregulation) is included. In the time step when the mineralization rate surpasses the immobilization,  $\delta[\text{N}_2\text{O}] > [\text{N}_2\text{O}]$ , and  $\text{N}_2\text{O}$  is lowered to  $10^{-23}$  M in three iterations as STOL 505 is met. In the next time step,  $\delta[\text{N}_2\text{O}] = \sim 10^{-13}$ , resulting in a scaling factor  $\lambda$  of  $10^{-10}$  that stops the simulation. Checking the calculations in the last iteration, the lower  $[\text{NH}_4^+]$  ( $2 \times 10^{-13}$  M) introduces a derivative ( $6.94 \times 10^{11}$ ) into the column of the Jacobian with respect to  $[\text{NH}_4^+]$ . Because

N<sub>2</sub>O production is a function of both immobilization and mineralization, a Monod substrate limiting function is added to downregulate the mineralization component (Eq. A5). In the row corresponding  
510 to [N<sub>2</sub>O], the off-diagonal terms are nonzero in the entries with respect to [NH<sub>4</sub><sup>+</sup>], [Lit1C], [Lit1N], and [SOM1]. Even though these values are relatively small because the fraction of net mineralization rate to produce [N<sub>2</sub>O] is small (0.02), inversion of the Jacobian matrix results in substantial values in the row, and the 10<sup>-13</sup> M update comes mainly from the entries with respect to Lit1C and Lit1N. This further illustrates that extremely small half saturation together with complex rate limiting formula  
515 can result in large derivatives at small concentration, which may lead to overshoot that results in a small update scaling factor.

### 4.3 CLM-PFLOTRAN simulations

We examine the nonphysical solution negativity in the coupled CLM-PFLOTRAN simulations for arctic (US-Brw), temperate (US-WBW), and tropical (BR-Cax) AmeriFlux sites. The CLM-PFLOTRAN  
520 simulations are run in the mode that PFLOTRAN only handles subsurface chemistry (decomposition, nitrification, denitrification, N plant uptake). For comparison, 1) depth and O<sub>2</sub> availability impact on decomposition, 2) cryoturbation, 3) SOM transport, and 4) nitrogen leaching are ignored by setting 1)  
525 decomp\_depth\_efolding to 10<sup>6</sup> m, o\_scalar to 1, 2) cryoturb\_diffusion, 3) som\_diffusion, and 4) sf\_no3 and sf\_sminn to 0. In the base case,  $k_m = 10^{-6}$  and residual concentration 10<sup>-15</sup>. Nitrogen is the focus as it is the rate limiting nutrient in CLM4.5 biogeochemistry. Spin-up simulations are used because they are generally more likely to face a nonphysical solution negativity because the simulations start far away from equilibrium. In these site simulations, PFLOTRAN uses the same 10  
530 layer grid for the 3.8 m one-dimensional column as CLM. The simulation duration is 500, 300, and 300 year for the arctic, temperate, and tropical sites as the system roughly reaches steady state within these simulation durations, and we do not experience different nonnegativity issues when simulation duration is longer.

#### 4.3.1 Site descriptions

The US-Brw site (71.35N, 156.62W) is located near Barrow, Alaska. The mean annual temperature, precipitation, and snowfall are -12 °C, 11 cm, and 69 cm, respectively (1971 ~ 2000) (Lara et al.,  
535 2012). The landscape is poorly drained polygonized tundra. The maximum thaw depth ranges from 30 to 40 cm, and the snow free-period is variable in length but generally begins in early June and lasts until early September (Hinkel and Nelson, 2003). The area is composed of several different representative wet-moist coastal sedge tundra types, including wet sedges, grasses, moss, and assorted lichens. The leaf area index (LAI) is ~ 1.1 (AmeriFlux data).

540 The US-WBW site (35.96N, 84.29W) is located in the Walker Branch Watershed in Oak Ridge, Tennessee (Hanson and Wullschleger, 2003). The climate is typical of the humid southern Appalachian region. The mean annual precipitation is ~ 139 cm, and the mean median temperature

is 14.5 °C. The soil is primarily Ultisols that developed in humid climates in the temperate zone on old or highly weathered material under forest. The temperate deciduous broadleaf forest was  
545 regenerated from agriculture land 50 years ago. LAI is ~ 6.2 (Hanson et al., 2004).

The BR-Cax site (-1.72N, -51.46W) is located in the eastern Amazon tropical rainforest. The mean annual rainfall is between 2000 and 2500 mm, with a pronounced dry season between June and November. The soil is a yellow oxisol (Brazilian classification latossolo amarelo) with a thick stony laterite layer at 3 ~ 4 m depth (da Costa et al., 2010). The vegetation is evergreen broadleaf  
550 forest. The LAI is 4 ~ 6 (Powell et al., 2013).

#### 4.3.2 Base case simulation results

For base case simulations, we use DC and LT because DC is the general geochemical modeling approach and is rigorous, and LT is less likely to cause numerical error than SU. The site climate data from 1998 to 2006, 2002 to 2010, and 2001 to 2006 are used to drive the spin-up simulation for the  
555 arctic (US-Brw), temperate (US-WBW), and tropical (BR-Cax) sites, respectively. This introduces a multi-year cycle in addition to the annual cycle (Figs. 7, 8, 9). Overall, CLM-PFLOTRAN is close to CLM4.5 in predicting LAI and nitrogen distribution among vegetation, litter, SOM,  $\text{NH}_4^+$  and  $\text{NO}_3^-$  pools for the arctic (Fig. 7), temperate (Fig. 8), and tropical site (Fig. 9). CLM4.5 does reach equilibrium earlier than CLM-PFLOTRAN as the latter represents slightly more inhibition on  
560 plant nitrogen uptake, depending on the half saturation. The impact is most obvious for LitN,  $\text{NH}_4^+$ , and  $\text{NO}_3^-$  in the tropical site (Fig. 9). This is expected as the nitrogen demand competition scheme implemented in CLM-PFLOTRAN is different from that in CLM4.5.

The arctic site shows a distinct summer growing season (Fig. 7): LAI and VEGN jump up at the beginning, then level off, and drop down at the end of the growing season when LITN jumps up due  
565 to litter fall.  $\text{NH}_4^+$  and  $\text{NO}_3^-$  drop to very low level at the beginning of growing season and accumulate at the other times. In addition to a longer growing season than the arctic site, the temperate site shows more litter fall by the end of the growing season as it is a temperate deciduous forest, which introduces immobilization demand that further lowers  $\text{NH}_4^+$  and  $\text{NO}_3^-$  concentrations (Fig. 8e inset). The seasonality is much less apparent in the tropical site than in the arctic and temperate sites. LAI,  
570 VEGN, LITN, and SOMN accumulate with less seasonal variations to reach an equilibrium. It takes much longer simulation duration to spin up the simulation for the arctic site than the temperate and tropical sites because the arctic site receives less solar radiation.

Except for the tropical site where the higher  $k_m$  of  $10^{-3}$  mol m $^{-3}$  results in lower immobilization, higher accumulation of LITN, and higher  $[\text{NH}_4^+]$  and  $[\text{NO}_3^-]$  during the spinup (Fig. 9), the range of  
575  $k_m$  values ( $10^{-3}$ ,  $10^{-6}$ , and  $10^{-9}$  mol m $^{-3}$ ) generally has limited impact on the overall calculations except that the nitrogen concentrations drop lower with lower  $k_m$  values (e.g., inset in Figs. 7e,f, 8e), which is similar to Fig. (6). The lack of sensitivity is because these very low concentrations do not make up a mass of nitrogen that is significant enough to influence the carbon and nitrogen cycle.

However, as a small  $k_m$  means weak downregulation and steep transition between zero order and  
580 first order, it has implications on accuracy, stability, and efficiency of the numerical solutions.

### 4.3.3 Efficiency

We use OIC (ORNL Institutional Cluster phase5 queue esd13q) for the comparison of computing time for the three sites using DC or DR with SU or LT. The results suggest that SU takes about 30~80% more time than CLM, and LT costs about two to four times that of CLM (Table 1). For LT  
585 with DC, the computing time increases with decreasing  $k_m$ . This is expected because a smaller  $k_m$  may require smaller time step size to march through steeper transition. The comparison between DC and DR is mixed. This is because DC has more complicated substrate limiting representation that requires smaller time step sizes to march through steep transitions, while DR has simpler substrate limiting representation, but a discontinuity that may require more iterations. We expect that CLM-  
590 PFLOTRAN will require more computational cost as more complex biogeochemical processes are represented, transport is added, and thermal hydrology (including freeze and thaw) are incorporated. Future code optimization for performance on next-generation supercomputers is expected to mitigate the computational cost issue.

### 4.3.4 Accuracy

595 CLM checks carbon and nitrogen mass balance for every time step, and report  $\geq 10^{-8} \text{ gm}^{-2}$  errors. Among our CLM-PFLOTRAN simulations, no mass balance error is recorded when LT is used. In contrast, when SU is used, mass balance errors are recorded for all of the simulations. We use the tropical site to demonstrate the accuracy issue by SU. With  $k_m = 10^{-3} \text{ mol m}^{-3}$ , the LAI, VEGN, LITN, SOMN,  $\text{NH}_4^+$ , and  $\text{NO}_3^-$  are similar to that calculated using LT (Fig. 9 vs. 10). With decreasing  $k_m$ , the results diverge by SU but not by LT. With  $k_m$  of  $10^{-6} \text{ mol m}^{-3}$ , much less nitrogen is  
600 predicted to accumulate with SU than with LT. Obviously, numerical error is introduced, and the error increases with decreasing  $k_m$ .

Looking into  $\text{NH}_4^+$  and  $\text{NO}_3^-$  concentration in the first year, SU calculation is similar to LT when  $\text{NH}_4^+$  and  $\text{NO}_3^-$  are abundant at early times (Fig. 11). As nitrogen becomes limiting at late times,  
605  $\text{NH}_4^+$  and  $\text{NO}_3^-$  accumulate lower by SU than by LT. Further looking into the daily cycles (Fig. 11 inset), plant uptake decreases  $\text{NH}_4^+$  and  $\text{NO}_3^-$  concentrations to very low level in the morning when photosynthesis starts; then the low concentration limits plant uptake, and nitrogen accumulates and rebounds until the next day. From day 226 to 230, SU calculations are only slightly lower than LT calculations during the rebound. From day 250 to 254, the SU calculated rebounds are about two  
610 orders of magnitude lower than LT calculations. From day 295 to 300, it worsens both in frequency and magnitude. Overall,  $\text{NH}_4^+$  and  $\text{NO}_3^-$  accumulation appear to be numerically “inhibited” when the system becomes increasingly nitrogen limiting and when SU is used. As a result, the mass balance error shots up during the nitrogen limiting periods (Fig. 12).

Further checking nitrogen dynamics between day 250 and 254, these "inhibited" intervals in Fig. 615 (11) coincide with the concentration valleys in the diagnostic species N<sub>2</sub>Od, which is used to track N<sub>2</sub>O production (reaction R11) due to decomposition (Eq. A5, Fig. 13). At the beginning of each CLM 0.5 h time step, we reset [N<sub>2</sub>Od] to 10<sup>-10</sup> in PFLTRAN so that it can be used to calculate the reaction rate for CLM (instead of saving concentration in previous time step) As we do not have any consumption reaction for N<sub>2</sub>Od, the decreases are purely numerical. The contribution of the 620 derivatives of the rate (Eq. A5) results in a large enough positive update to N<sub>2</sub>Od, which results in a small scaling factor, and the solution is considered converged due to less than STOL update. This small scaling factor and false convergence result in the "inhibition" of NH<sub>4</sub><sup>+</sup> and NO<sub>3</sub><sup>-</sup> production, and manifest as much less nitrogen accumulation in Fig. (10). Decreasing STOL and/or  $\lambda_{min}$  does not resolve the issue (Fig. (11)), nor does removing these diagnostic species, and/or decreasing  $\alpha$  625 (say from 0.99 to 0.5). As long as there are low concentrations, e.g., NH<sub>4</sub><sup>+</sup>, NO<sub>3</sub><sup>-</sup>, it is possible to have a sufficiently large update to result in a small scaling factor to "inhibit" production.

#### 4.3.5 Stability and robustness

PFLTRAN may stop CLM-PFLTRAN run due to 1) too small a scaling factor for SU to avoid excessive numerical error, 2) too small a time step size or too many time step cuts for either SU or 630 LT, and 3) singular Jacobian matrix for LT.

With SU and DC, the simulations run to conclusion for  $k_m = 10^{-3}, 10^{-6}$ , and  $10^{-9} \text{ mol m}^{-3}$  but abort for  $k_m = 10^{-12}$  for all of the three sites. The reasons for the unfinished runs are too small a scaling factor for NO<sub>3</sub><sup>-</sup>. As indicated in Test 3, it is not surprising to see positive updates to NO<sub>3</sub><sup>-</sup> as they depend on source and sink terms not only for NO<sub>3</sub><sup>-</sup> but also for NH<sub>4</sub><sup>+</sup> because of the nitrogen 635 demand distribution scheme (Eq. 20) for plant uptake and immobilization. With smaller  $k_m$ , the derivative of the substrate limiting function becomes bigger when the concentration is lower, and the off-diagonal entries in the Jacobian matrix become more dominant, increasing the probability of producing positive update. When a greater than [NO<sub>3</sub><sup>-</sup>] update is produced, [NO<sub>3</sub><sup>-</sup>] is expected to decrease by  $1-\alpha$  times (0.01 by default) for each subsequent iterations, making it lower than the 640 residual concentration ( $10^{-15}$ ). If the  $\lambda$  is not greater than  $10^{-10}$ , and the solution may be considered converged because STOL is satisfied, [NO<sub>3</sub><sup>-</sup>] can be very low, much below residual concentration ( $10^{-26}$ ). With such low concentrations, a positive update can make the scaling factor to be less than  $10^{-10}$ . The arctic site simulation aborts at a much later time than the temperate and tropical site because the uptake and immobilization rate is much smaller in the former site.

645 A lower STOL can be used to avoid or mitigate the false convergence. With STOL =  $10^{-12}$ , the simulations abort for  $k_m = 10^{-3}, 10^{-6}$ , and  $10^{-9} \text{ mol m}^{-3}$  for the three sites due to too big an update for the diagnostic variables (PlantN, DeniN, or N<sub>2</sub>Od). Instead of aborting the run when the scaling factor is less than the minimum allowable value  $\lambda_{min}$ , an alternative is to consider the iteration diverges and return to the time stepping subroutine to cut time step size to increase accuracy. This

650 mitigates the stability and accuracy challenge at the expense of computing time. Our results show the default  $\lambda_{min} = 10^{-10}$  can result in excessive error even when STOL is extremely small. It is not clear how large a  $\lambda_{min}$  value can insure accuracy without introducing unnecessary computing time. For this reason, we caution against use of SU.

Similar to SU, the simulations using LT run to conclusion for  $k_m = 10^{-3}, 10^{-6}$ , and  $10^{-9} \text{ mol m}^{-3}$  655 but abort for  $k_m = 10^{-12}$  for the three sites. The runs abort at 21.6, 2.46, and 1.1 year for the arctic, temperate, and tropical site because the number of time step cuts for one time step exceeds MAX\_CUT = 16 (default). Increasing MAX\_CUT to 50, the simulations run to conclusion with longer computing time (Table 1). Looking into the reason for time step cuts, it usually involves iteration with  $\text{NO}_3^-$  concentration oscillation between the first order and zero order (Fig. 15b, for 660 example, between  $1.69 \times 10^{-11}$  and  $1.14 \times 10^{-13}$  in the sixth layer in 0.5 year for BR-Cax site). While requiring a large MAX\_CUT, all of the simulations conclude with less than a 20% increase of computing time for  $k_m$  of  $10^{-12}$  over  $10^{-9}$ . These results suggest that log transformation together with downregulation with reasonable half saturation and residual concentration can provide accurate, stable, and feasibly efficient solutions for CLM-PFLOTRAN biogeochemistry simulations.

## 665 5 Summary and Conclusions

We implement CLM-CN decomposition cascadec, nitrification, denitrification, and plant nitrogen uptake reactions in CLM-PFLOTRAN. As CLM uses explicit time stepping and demand-based competition, the concentration is always nonnegative. PFLOTRAN uses implicit time stepping and Newton-Raphson method; the concentration can become negative, which is not physical, may cause 670 numerical instability, and introduce numerical error.

Both scaling back update in each iteration and log transformation can enforce nonnegativity. SU allows large time step sizes to achieve efficiency, but may introduce excessive numerical error if the scaling factor is small and the iterations are considered converged due to small updates. Log transformation involves multiplication of the Jacobian matrix by the concentration vector, decreasing 675 the condition number by orders of magnitude as the concentration can be low. As a result, LT often decreases the time step size and increases computational cost. Neither SU nor LT prevents too small or 0 concentrations. When the concentration becomes too small and essentially 0, SU may stop all reactions by a small positivity update caused by consumption, numerical overshoot, or truncation error and LT can fail due to too stiff or singular Jacobian matrix. Both SU and LT require that 680 the limitation of reactant availability on reaction rates to be represented such that solution to the mathematical representation does not introduce negative or 0 concentrations.

The first-order rate accounts for limitation of the reactant availability on the reaction rate, and the solution is nonnegative. Adding a residual concentration makes it positive. For the zero-order rate (the rate is not a function of a reactant), the Monod substrate limiting function provides a smooth

685 transition from a zero order when the reactant is abundant to a first order when the reactant becomes limiting. The downregulation relaxes with decreasing half saturation and residual concentration and disappears when both are 0.

Our CLM-PFLOTRAN spin-up simulation at an arctic, temperate, and tropical site indicates that accurate and stable solution can be achieved with log transformation with two to three times the  
690 computing time of CLM4.5 for a range of half saturation values from  $10^{-3}$  to  $10^{-9}$  and a residual concentration of  $10^{-15}$  for nitrogen. With half saturation of  $10^{-12}$ , the number of maximum time cuts has to be increased from the default 16 to accommodate for small time step sizes to resolve  
695 small concentration changes in the transition of zero and first-order rate. The computing time increase from the half saturation of  $10^{-12}$  to  $10^{-9}$  is less than 20%. As physical half saturation ranges from  $10^{-5}$  to  $10^{-6}$  M for nitrogen, and the detection limits are often above  $10^{-9}$  M, log transformation together with downregulation by reasonable half saturation and residual concentration is expected to provide an accurate, stable, and efficient solution for CLM-PFLOTRAN implementation  
700 for current CLM biogeochemistry. As more substrate limiting processes, such as labile C, P, O<sub>2</sub>, and H<sub>2</sub>, are implemented with lower half saturation and residual concentration, and more complicated rate relationship, the maximum allowable time step cut may need to be increased, and the computing time is expected to increase.

## 6 Code availability

PFLOTRAN is an open-source software. It is distributed under the terms of the GNU Lesser General Public License as published by the Free Software Foundation either version 2.1 of the License, or  
705 any later version. It is available at <https://bitbucket.org/pfotran>.

CLM-PFLOTRAN is currently under development and will be available subject to guidelines of NGEE-Arctic and ACME projects.

## 7 Author contribution

G. B., B. A., R. M., J. K., and F. H. developed the CLM-PFLOTRAN framework that this work  
710 built upon. F.Y., G.T., G. B., and X.X. added biogeochemistry to the CLM-PFLOTRAN interface. F. Y. proposed the nitrification and denitrification reactions and rate formulae. G. T., F. Y., and X. X. implemented the CLM biogeochemistry in PFLOTRAN under guidance of G. H., P. L., S. P., and P.T. G.T. prepared the manuscript with contributions from all co-authors. G. T., F. Y., G. B., and G.H. contributed equally to the work.

715 *Acknowledgements.* Thanks to Nathaniel O. Collier at ORNL for many discussion that contributed significantly to this work. Thanks to Kathie Tallant and Cathy Jones at ORNL for editing service. This research was funded by

the U.S. Department of Energy, Office of Sciences, Biological and Environmental Research, Terrestrial Ecosystem Sciences and Subsurface Biogeochemical Research Program, and is a product of the Next-Generation Ecosystem Experiments in the Arctic (NGEE-Arctic) project. ORNL is managed by UT-Battelle, LLC, for the  
720 U.S. Department of Energy under contract DE-AC05-00OR22725.

## References

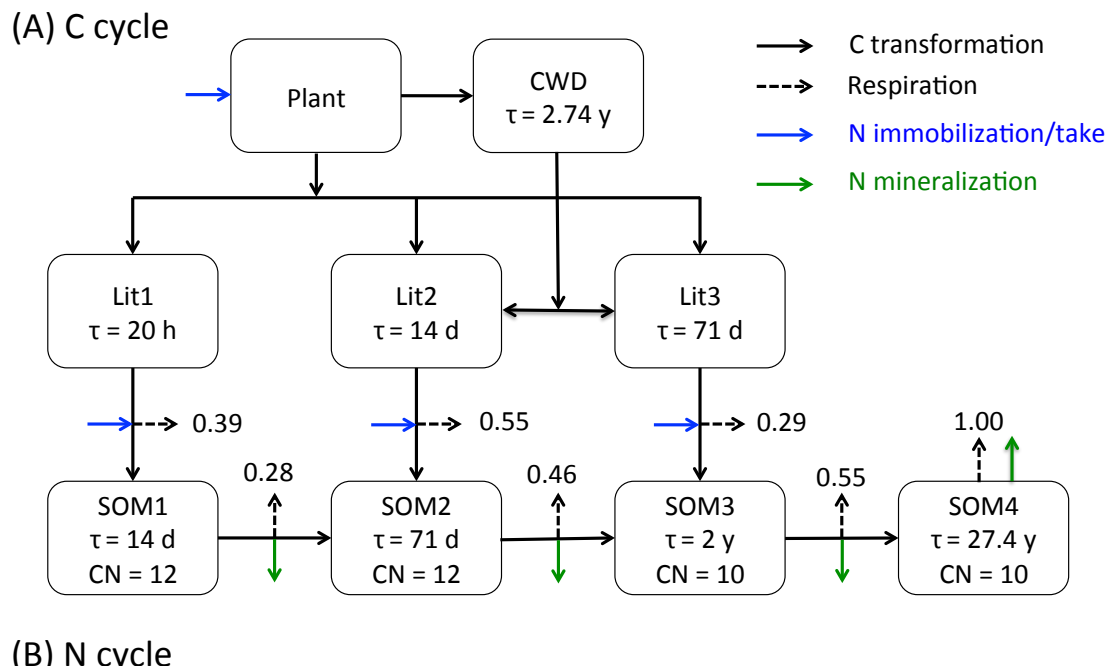
- Antonelli, L., Briani, M., D'Ambra, P., and Fraioli, V.: Positivity Issues in Adaptive Solutions of Detailed Chemical Schemes for Engine Simulations, in: Communications to SIMAI Congress, vol. 3, pp. 303.1–303.12, 2009.
- 725 Bethke, C. M.: Geochemical and biogeochemical reaction modeling, Cambridge University Press, 2007.
- Bonan, G. B., Hartman, M. D., Parton, W. J., and Wieder, W. R.: Evaluating litter decomposition in earth system models with long-term litterbag experiments: an example using the Community Land Model version 4 (CLM4), *Global Change Biology*, pp. 957–974, doi:10.1111/gcb.12031, <http://dx.doi.org/10.1111/gcb.12031>, 2012.
- 730 Boyer, E. W., Alexander, R. B., Parton, W. J., Li, C., Butterbach-Bahl, K., Donner, S. D., Skaggs, R. W., and Grosso, S. J. D.: Modeling Denitrification In Terrestrial And Aquatic Ecosystems At Regional Scales, *Ecological Applications*, 16, 2123–2142, doi:10.1890/1051-0761(2006)016, [http://dx.doi.org/10.1890/1051-0761\(2006\)016](http://dx.doi.org/10.1890/1051-0761(2006)016), 2006.
- 735 Broekhuizen, N., Rickard, G. J., Bruggeman, J., and Meister, A.: An improved and generalized second order, unconditionally positive, mass conserving integration scheme for biochemical systems, *Applied Numerical Mathematics*, 58, 319–340, doi:10.1016/j.apnum.2006.12.002, <http://www.sciencedirect.com/science/article/pii/S0168927406002224>, 2008.
- 740 Bruggeman, J., Burchard, H., Kooi, B. W., and Sommeijer, B.: A second-order, unconditionally positive, mass-conserving integration scheme for biochemical systems, *Applied Numerical Mathematics*, 57, 36–58, doi:10.1016/j.apnum.2005.12.001, <http://www.sciencedirect.com/science/article/pii/S0168927405002242>, 2007.
- 745 Burchard, H., Deleersnijder, E., and Meister, A.: A high-order conservative Patankar-type discretisation for stiff systems of production–destruction equations, *Applied Numerical Mathematics*, 47, 1–30, doi:10.1016/S0168-9274(03)00101-6, <http://www.sciencedirect.com/science/article/pii/S0168927403001016>, 2003.
- Burchard, H., Deleersnijder, E., and Meister, A.: Application of modified Patankar schemes to stiff biogeochemical models for the water column, *Ocean Dynamics*, 55, 326–337, doi:10.1007/s10236-005-0001-x, <http://link.springer.com/article/10.1007%2Fs10236-005-0001-x>, 2005.
- Chapin, F., Matson, P., and Vitousek, P.: Principles of Terrestrial Ecosystem Ecology, Springer, 2011.
- 750 Chen, D. and Plemmons, R. J.: Nonnegativity constraints in numerical analysis, in: *Symposium on the Birth of Numerical Analysis*, pp. 109–140, 2009.
- da Costa, A. C. L., Galbraith, D., Almeida, S., Portela, B. T. T., da Costa, M., de Athaydes Silva Junior, J., Braga, A. P., de Gonçalves, P. H. L., de Oliveira, A. A. R., Fisher, R., Phillips, O. L., Metcalfe, D. B., Levy, P., and Meir, P.: Effect of 7 yr of experimental drought on vegetation dynamics and biomass storage of an eastern Amazonian rainforest, *New Phytologist*, 187, 579–591, doi:10.1111/j.1469-8137.2010.03309.x, <http://dx.doi.org/10.1111/j.1469-8137.2010.03309.x>, 2010.
- Dickinson, R. E., Berry, J. A., Bonan, G. B., Collatz, G. J., Field, C. B., Fung, I. Y., Goulden, M., Hoffmann, W. A., Jackson, R. B., Myneni, R., Sellers, P. J., and Shaikh, M.: Nitrogen Controls on Climate Model Evapotranspiration, *Journal of Climate*, 15, 278–295, doi:10.1175/1520-0442(2002)015, [http://dx.doi.org/10.1175/1520-0442\(2002\)015](http://dx.doi.org/10.1175/1520-0442(2002)015), 2002.

- Eltrop, L. and Marschner, H.: Growth and mineral nutrition of non-mycorrhizal and mycorrhizal Norway spruce (*Picea abies*) seedlings grown in semi-hydroponic sand culture, *New Phytologist*, 133, 469–478, doi:10.1111/j.1469-8137.1996.tb01914.x, <http://dx.doi.org/10.1111/j.1469-8137.1996.tb01914.x>, 1996.
- Falkengren-Grerup, U.: Interspecies differences in the preference of ammonium and nitrate in vascular plants, 765 *Oecologia*, 102, 305–311, doi:10.1007/BF00329797, <http://dx.doi.org/10.1007/BF00329797>, 1995.
- Fang, Y., Huang, M., Liu, C., Li, H., and Leung, L. R.: A generic biogeochemical module for Earth system models: Next Generation BioGeoChemical Module (NGBGC), version 1.0, *Geosci. Model Dev.*, 6, 1977–1988, doi:10.5194/gmd-6-1977-2013, <http://www.geosci-model-dev.net/6/1977/2013>, gMD, 2013.
- Fennell, D. E. and Gossett, J. M.: Modeling the Production of and Competition for Hydrogen in a Dechlorinating 770 Culture, *Environmental Science & Technology*, 32, 2450–2460, doi:10.1021/es980136l, <http://pubs.acs.org/doi/pdfplus/10.1021/es980136l>, 1998.
- Foulland, E., Gosselin, M., Rivkin, R. B., Vasseur, C., and Mostajir, B.: Nitrogen uptake by heterotrophic bacteria and phytoplankton in Arctic surface waters, *Journal of Plankton Research*, 29, 369–376, <http://plankt.oxfordjournals.org/content/29/4/369.abstract>, 2007.
- Gherardi, L. A., Sala, O. E., and Yahdjian, L.: Preference for different inorganic nitrogen forms among plant 775 functional types and species of the Patagonian steppe, *Oecologia*, 173, 1075–1081, doi:10.1007/s00442-013-2687-7, <http://dx.doi.org/10.1007/s00442-013-2687-7>, 2013.
- Grant, R. F.: Modelling changes in nitrogen cycling to sustain increases in forest productivity under elevated atmospheric CO<sub>2</sub> and contrasting site conditions, *Biogeosciences*, 10, 7703–7721, doi:10.5194/bg-10-7703-780 2013, <http://www.biogeosciences.net/10/7703/2013>, bG, 2013.
- Gu, C. and Riley, W. J.: Combined effects of short term rainfall patterns and soil texture on soil nitrogen cycling — A modeling analysis, *Journal of Contaminant Hydrology*, 112, 141–154, doi:10.1016/j.jconhyd.2009.12.003, <http://www.sciencedirect.com/science/article/pii/S0169772209001648>, 2010.
- Hammond, G. E.: Innovative Methods for Solving Multicomponent Biogeochemical groundwater Transport on 785 Supercomputers, Thesis, University of Illinois at Urbana-Champaign, 2003.
- Hanson, P. and Wullschleger, S.: North American Temperate Deciduous Forest Responses to Changing Precipitation Regimes, Springer Verlag, 2003.
- Hanson, P. J., Amthor, J. S., Wullschleger, S. D., Wilson, K. B., Grant, R. F., Hartley, A., Hui, D., Hunt, J. 790 E. R., Johnson, D. W., Kimball, J. S., King, A. W., Luo, Y., McNulty, S. G., Sun, G., Thornton, P. E., Wang, S., Williams, M., Baldocchi, D. D., and Cushman, R. M.: Oak forest carbon and water simulations: model intercomparisons and evaluations against independent data, *Ecological Monographs*, 74, 443–489, doi:10.1890/03-4049, <http://www.esajournals.org/doi/pdf/10.1890/03-4049>, 2004.
- Hinkel, K. M. and Nelson, F. E.: Spatial and temporal patterns of active layer thickness at Circumpolar Active 795 Layer Monitoring (CALM) sites in northern Alaska, 1995–2000, *Journal of Geophysical Research: Atmospheres*, 108, 8168, doi:10.1029/2001JD000927, <http://dx.doi.org/10.1029/2001JD000927>, 2003.
- Hungate, R.: The rumen microbial ecosystem, *Annual Review of Ecology and Systematics*, pp. 39–66, 1975.
- HØGh-Jensen, H., Wollenweber, B., and Schjoerring, J. K.: Kinetics of nitrate and ammonium absorption and accompanying H<sup>+</sup> fluxes in roots of *Lolium perenne* L. and N<sub>2</sub>-fixing *Trifolium repens* L, *Plant, Cell & Envi-*

- 800 ronment, 20, 1184–1192, doi:10.1046/j.1365-3040.1997.d01-145.x, <http://dx.doi.org/10.1046/j.1365-3040.1997.d01-145.x>, 1997.
- IPCC: Climate Change 2013: The Physical Science Basis. Contribution of Working Group I to the Fifth Assessment Report of the Intergovernmental Panel on Climate Change, Cambridge University Press, Cambridge, United Kingdom and New York, NY, USA, doi:10.1017/CBO9781107415324, [www.climatechange2013.org](http://www.climatechange2013.org), 2013.
- 805 Jarrell, K. F.: Extreme Oxygen Sensitivity in Methanogenic Archaeabacteria, *BioScience*, 35, 298–302, <http://bioscience.oxfordjournals.org/content/35/5/298.abstract>, 1985.
- Kamer, K., Kennison, R. L., and Fong, P.: Rates of inorganic nitrogen uptake by the estuarine green macroalgae *Enteromorpha intestinalis* and *Ulva expansa*, vol. 2003, pp. 130–141, 2001.
- 810 Kirchman, D. L.: The uptake of inorganic nutrients by heterotrophic bacteria, *Microbial Ecology*, 28, 255–271, doi:10.1007/BF00166816, <http://dx.doi.org/10.1007/BF00166816>, 1994.
- Kirchman, D. L. and Wheeler, P. A.: Uptake of ammonium and nitrate by heterotrophic bacteria and phytoplankton in the sub-Arctic Pacific, *Deep Sea Research Part I: Oceanographic Research Papers*, 45, 347–365, doi:10.1016/S0967-0637(97)00075-7, <http://www.sciencedirect.com/science/article/pii/S0967063797000757>, 1998.
- 815 Kuzyakov, Y. and Xu, X.: Competition between roots and microorganisms for nitrogen: mechanisms and ecological relevance, *New Phytologist*, 198, 656–669, doi:10.1111/nph.12235, <http://dx.doi.org/10.1111/nph.12235>, 2013.
- Lara, M. J., Villarreal, S., Johnson, D. R., Hollister, R. D., Webber, P. J., and Tweedie, C. E.: Estimated change 820 in tundra ecosystem function near Barrow, Alaska between 1972 and 2010, *Environmental Research Letters*, 7, 015 507, 2012.
- Lichtner, P. C., Hammond, G. E., Lu, C., Karra, S., Bisht, G., Andre, B., Mills, R. T., and Jitu, K.: PFLO-TRAN User Manual: A Massively Parallel Reactive Flow and Transport Model for Describing Surface and Subsurface Processes, Report, 2015.
- 825 Maggi, F., Gu, C., Riley, W. J., Hornberger, G. M., Venterea, R. T., Xu, T., Spycher, N., Steefel, C., Miller, N. L., and Oldenburg, C. M.: A mechanistic treatment of the dominant soil nitrogen cycling processes: Model development, testing, and application, *Journal of Geophysical Research: Biogeosciences*, 113, G02 016, doi:10.1029/2007JG000578, <http://dx.doi.org/10.1029/2007JG000578>, 2008.
- Manzoni, S. and Porporato, A.: Soil carbon and nitrogen mineralization: Theory and models across scales, *Soil 830 Biology and Biochemistry*, 41, 1355–1379, doi:10.1016/j.soilbio.2009.02.031, <http://www.sciencedirect.com/science/article/pii/S0038071709000765>, 2009.
- Middelburg, J. J. and Nieuwenhuize, J.: Nitrogen uptake by heterotrophic bacteria and phytoplankton in the nitrate-rich Thames estuary, *Marine Ecology Progress Series*, 203, 13–21, <http://www.int-res.com/abstracts/meps/v203/p13-21/>, 2000.
- 835 Nollet, L. M. L. and De Gelder, L. S. P.: *Handbook of Water Analysis* (3rd Edition), CRC Press, 2013.
- Nordin, A., Högberg, P., and Näsholm, T.: Soil nitrogen form and plant nitrogen uptake along a boreal forest productivity gradient, *Oecologia*, 129, 125–132, doi:10.1007/s004420100698, <http://dx.doi.org/10.1007/s004420100698>, 2001.

- Oleson, K., Lawrence, D., Bonan, G., Levis, S., Swenson, S., Thornton, P., Bozbayik, A., Fisher, R., Heald, C.,  
 840 Kluzek, E., Lamarque, J.-F., Lawrence, P., Lipscomb, W., Muszala, S., and Sacks, W.: Technical description  
 of version 4.5 of the Community Land Model (CLM), Ncar/tn-503+str, ncar technical note, NCAR,  
 doi:10.5065/D6RR1W7M, [http://www.cesm.ucar.edu/models/cesm1.2/clm/CLM45\\_Tech\\_Note.pdf](http://www.cesm.ucar.edu/models/cesm1.2/clm/CLM45_Tech_Note.pdf), 2013.
- Parkhurst, D. L. and Appelo, C.: User's guide to PHREEQC (Version 2): A computer program for speciation,  
 batch-reaction, one-dimensional transport, and inverse geochemical calculations, Water-Resources Investigations  
 845 99-4259, USGS, 1999.
- Parton, W. J., Mosier, A. R., Ojima, D. S., Valentine, D. W., Schimel, D. S., Weier, K., and Kulmala, A. E.:  
 Generalized model for N2 and N2O production from nitrification and denitrification, Global Biogeochemical  
 Cycles, 10, 401–412, doi:10.1029/96GB01455, <http://dx.doi.org/10.1029/96GB01455>, 1996.
- Parton, W. J., Holland, E. A., Del Gross, S. J., Hartman, M. D., Martin, R. E., Mosier, A. R., Ojima, D. S., and  
 850 Schimel, D. S.: Generalized model for NO x and N2O emissions from soils, Journal of Geophysical Research:  
 Atmospheres, 106, 17 403–17 419, doi:10.1029/2001JD900101, <http://dx.doi.org/10.1029/2001JD900101>,  
 2001.
- Pfautsch, S., Rennenberg, H., Bell, T. L., and Adams, M. A.: Nitrogen uptake by Eucalyptus regnans and  
 Acacia spp. – preferences, resource overlap and energetic costs, Tree Physiology, 29, 389–399, <http://treephys.oxfordjournals.org/content/29/3/389.abstract>, 2009.
- Pierre, M. and Schmitt, D.: Blowup in Reaction-Diffusion Systems with Dissipation of Mass, SIAM Review,  
 42, 93–106, doi:10.1137/S0036144599359735, <http://dx.doi.org/10.1137/S0036144599359735><http://epubs.siam.org/doi/abs/10.1137/S0036144599359735>, 2000.
- Powell, T. L., Galbraith, D. R., Christoffersen, B. O., Harper, A., Imbuzeiro, H. M. A., Rowland, L., Almeida, S.,  
 860 Brando, P. M., da Costa, A. C. L., Costa, M. H., Levine, N. M., Malhi, Y., Saleska, S. R., Sotta, E., Williams,  
 M., Meir, P., and Moorcroft, P. R.: Confronting model predictions of carbon fluxes with measurements of  
 Amazon forests subjected to experimental drought, New Phytologist, 200, 350–365, doi:10.1111/nph.12390,  
<http://dx.doi.org/10.1111/nph.12390>, 2013.
- Riley, W. J., Maggi, F., Kleber, M., Torn, M. S., Tang, J. Y., Dwivedi, D., and Guerry, N.: Long residence times  
 865 of rapidly decomposable soil organic matter: application of a multi-phase, multi-component, and vertically  
 resolved model (BAMS1) to soil carbon dynamics, Geosci. Model Dev., 7, 1335–1355, doi:10.5194/gmd-7-  
 1335-2014, <http://www.geosci-model-dev.net/7/1335/2014/>, gMD, 2014.
- Schmidt, M. W. I., Torn, M. S., Abiven, S., Dittmar, T., Guggenberger, G., Janssens, I. A., Kleber, M., Kogel-  
 Knabner, I., Lehmann, J., Manning, D. A. C., Nannipieri, P., Rasse, D. P., Weiner, S., and Trumbore, S. E.:  
 870 Persistence of soil organic matter as an ecosystem property, Nature, 478, 49–56, <http://dx.doi.org/10.1038/nature10386>, 10.1038/nature10386, 2011.
- Sellers, P. J., Dickinson, R. E., Randall, D. A., Betts, A. K., Hall, F. G., Berry, J. A., Collatz, G. J., Denning,  
 A. S., Mooney, H. A., Nobre, C. A., Sato, N., Field, C. B., and Henderson-Sellers, A.: Modeling the Ex-  
 changes of Energy, Water, and Carbon Between Continents and the Atmosphere, Science, 275, 502–509,  
 875 doi:10.1126/science.275.5299.502, <http://www.sciencemag.org/content/275/5299/502.abstract>, 1997.
- Seneviratne, S. I., Corti, T., Davin, E. L., Hirschi, M., Jaeger, E. B., Lehner, I., Orlowsky, B., and Teuling,  
 A. J.: Investigating soil moisture–climate interactions in a changing climate: A review, Earth-Science Re-

- views, 99, 125–161, doi:10.1016/j.earscirev.2010.02.004, <http://www.sciencedirect.com/science/article/pii/S0012825210000139>, 2010.
- 880 Shampine, L. F., Thompson, S., Kierzenka, J. A., and Byrne, G. D.: Non-negative solutions of ODEs, Applied Mathematics and Computation, 170, 556–569, doi:<http://dx.doi.org/10.1016/j.amc.2004.12.011>, <http://www.sciencedirect.com/science/article/pii/S0096300304009683>, 2005.
- Steefel, C. I., Appelo, C. A. J., Arora, B., Jacques, D., Kalbacher, T., Kolditz, O., Lagneau, V., Lichtner, P. C., Mayer, K. U., Meeussen, J. C. L., Molins, S., Moulton, D., Shao, H., Šimůnek, J., Spycher, N., Yabusaki, S. B., and Yeh, G. T.: Reactive transport codes for subsurface environmental simulation, Computational Geosciences, pp. 1–34, doi:10.1007/s10596-014-9443-x, <http://dx.doi.org/10.1007/s10596-014-9443-x>, 2014.
- 885 Tang, G., Watson, D. B., Wu, W.-M., Schadt, C. W., Parker, J. C., and Brooks, S. C.: U(VI) Bioreduction with Emulsified Vegetable Oil as the Electron Donor – Model Application to a Field Test, Environmental Science & Technology, 47, 3218–3225, doi:10.1021/es304643h, <http://dx.doi.org/10.1021/es304643h>, 2013a.
- 890 Tang, J., Riley, W., Koven, C., and Subin, Z.: CLM4-BeTR, a generic biogeochemical transport and reaction module for CLM4: model development, evaluation, and application, Geoscientific Model Development, 6, 127–140, 2013b.
- Tang, J. Y. and Riley, W. J.: Technical Note: A generic law-of-the-minimum flux limiter for simulating substrate limitation in biogeochemical models, Biogeosciences Discuss., 12, 13 399–13 425, doi:10.5194/bgd-895 12-13399-2015, <http://www.biogeosciences-discuss.net/12/13399/2015/>, bGD, 2015.
- Thornton, P. E. and Rosenbloom, N. A.: Ecosystem model spin-up: Estimating steady state conditions in a coupled terrestrial carbon and nitrogen cycle model, Ecological Modelling, 189, 25–48, doi:10.1016/j.ecolmodel.2005.04.008, <http://www.sciencedirect.com/science/article/pii/S0304380005001948>, 2005.
- 900 Veuger, B., Middelburg, J. J., Boschker, H. T. S., Nieuwenhuize, J., van Rijswijk, P., Rochelle-Newall, E. J., and Navarro, N.: Microbial uptake of dissolved organic and inorganic nitrogen in Randers Fjord, Estuarine, Coastal and Shelf Science, 61, 507–515, doi:10.1016/j.ecss.2004.06.014, <http://www.sciencedirect.com/science/article/pii/S0272771404001593>, 2004.
- 905 Wang, G., Post, W. M., and Mayes, M. A.: Development of microbial-enzyme-mediated decomposition model parameters through steady-state and dynamic analyses, Ecological Applications, 23, 255–272, doi:10.1890/12-0681.1, <http://dx.doi.org/10.1890/12-0681.1><http://www.esajournals.org/doi/abs/10.1890/12-0681.1>, 2012.
- Warren, C. R. and Adams, P. R.: Uptake of nitrate, ammonium and glycine by plants of Tasmanian wet eucalypt forests, Tree Physiology, 27, 413–419, <http://treephys.oxfordjournals.org/content/27/3/413.abstract>, doi:10.1093/treephys/27.3.413, 2007.
- 910 Xu, T., Sonnenthal, E., Spycher, N., and Pruess, K.: TOUGHREACT—A simulation program for non-isothermal multiphase reactive geochemical transport in variably saturated geologic media: Applications to geothermal injectivity and CO<sub>2</sub> geological sequestration, Computers & Geosciences, 32, 145–165, doi:10.1016/j.cageo.2005.06.014, <http://www.sciencedirect.com/science/article/pii/S0098300405001500>, 2006.



(B) N cycle

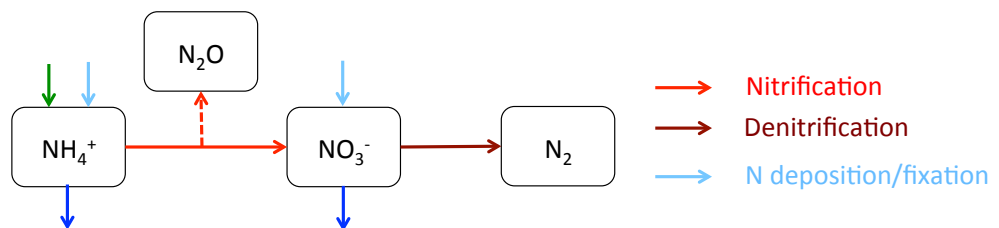


**Figure 1.** The reaction network for the carbon (A) and nitrogen (B) cycles implemented in this work. The carbon cycle is modified from Thornton and Rosenbloom (2005) and Bonan et al. (2012).  $\tau$  is the turnover time, and CN is the CN ratio in gC over gN.

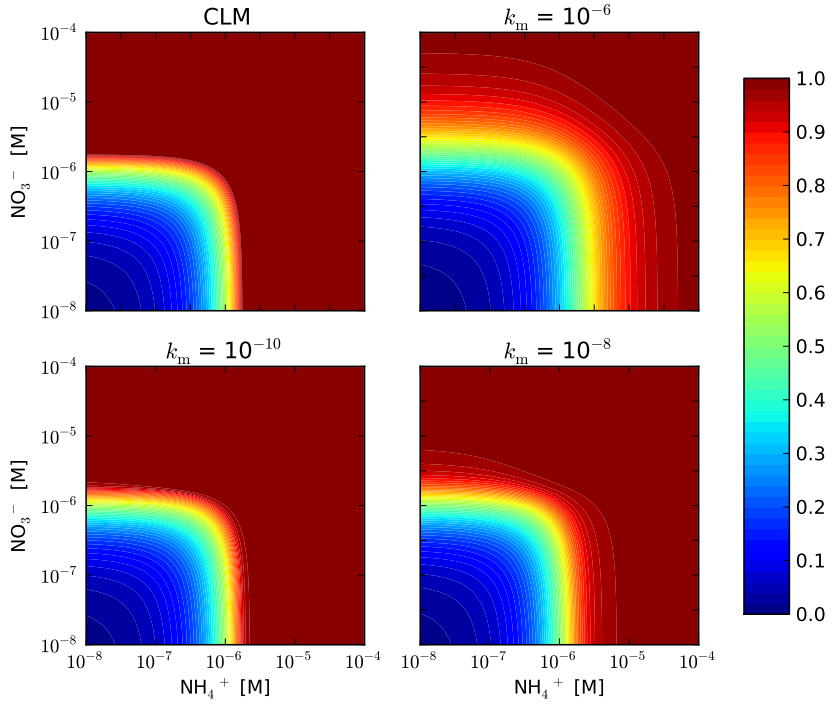


**Figure 2.** The ratio of uptake and demand ( $f_{pi}$ ) as a function of concentrations with CLM and representation by Eqs. (19) and (20) in a 0.5 h time step with an uptake rate of  $10^{-9} \text{ M s}^{-1}$ .  $f_{pi}$  for the new representation is less than or equal to that for CLM. The difference decreases with decreasing half saturation  $k_m$ .

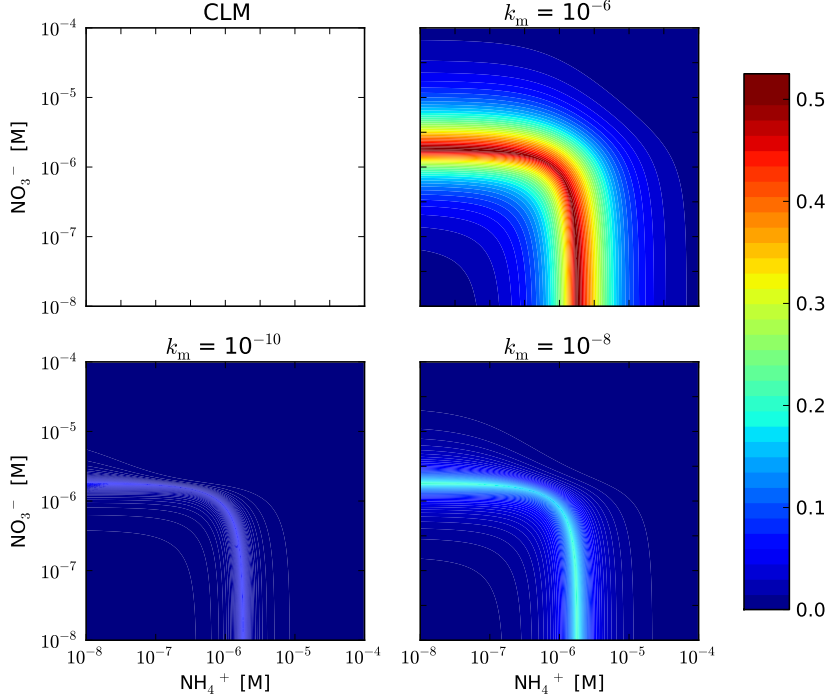


**Figure 3.** The difference plots for Fig. (2).

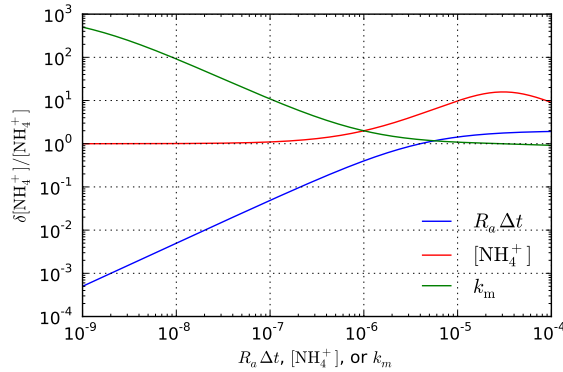


**Figure 4.** The calculated ratio of update over concentration for the first iteration as a function of time step size ( $R_a \Delta t$ ), initial concentration ( $\text{NH}_4^+$ ), and half saturation ( $k_m$ ) for solving  $d[\text{NH}_4^+]/dt = -R_a[\text{NH}_4^+]/(\text{NH}_4^+ + k_m)$  using the backward Euler method and Newton-Raphson method. Without scaling back the update ( $\delta$ ), the concentration in the first iteration step ( $[\text{NH}_4^+]^{k+1,1}$ ) can go negative if  $R_a \Delta t > 10^{-5}$ ,  $[\text{NH}_4^+]^k > 10^{-6}$ , or  $k_m < 10^{-6}$ . Unless specified in the figure, the base case parameters are  $R_a \Delta t = 10^{-3}$ ,  $\text{NH}_4^+ = 10^{-6}$ , and  $k_m = 10^{-6}$ .

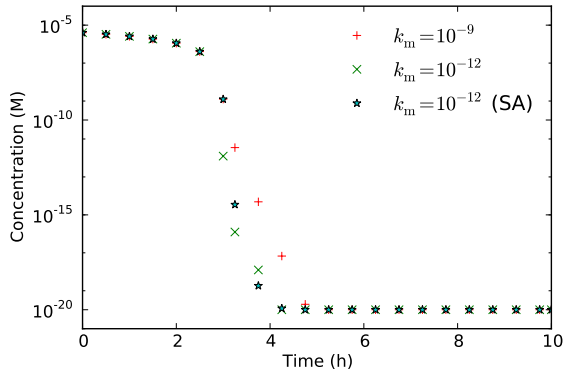


**Figure 5.** Influence of half saturation ( $k_m$ ) on the simulated  $\text{NH}_4^+$  concentration decrease due to plant uptake. Too small a half saturation may result in false convergence due to too small an update (scaling factor) during the iteration. The semi-analytical (SA) solution (Eq. D2) is used for comparison.

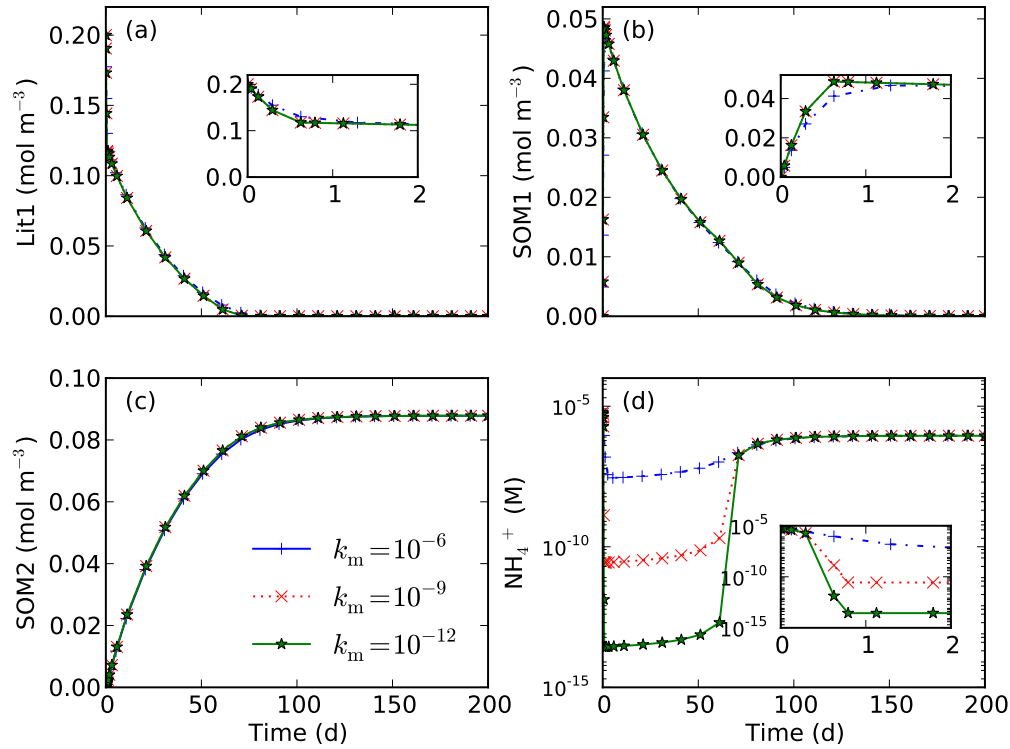


**Figure 6.** Influence of half saturation  $k_m$  on decomposition that involves both nitrogen immobilization and mineralization. Smaller half saturation can result in lower nitrogen concentration (d) but does not substantially impact the calculated concentrations other than  $\text{NH}_4^+$  (a,b,c).

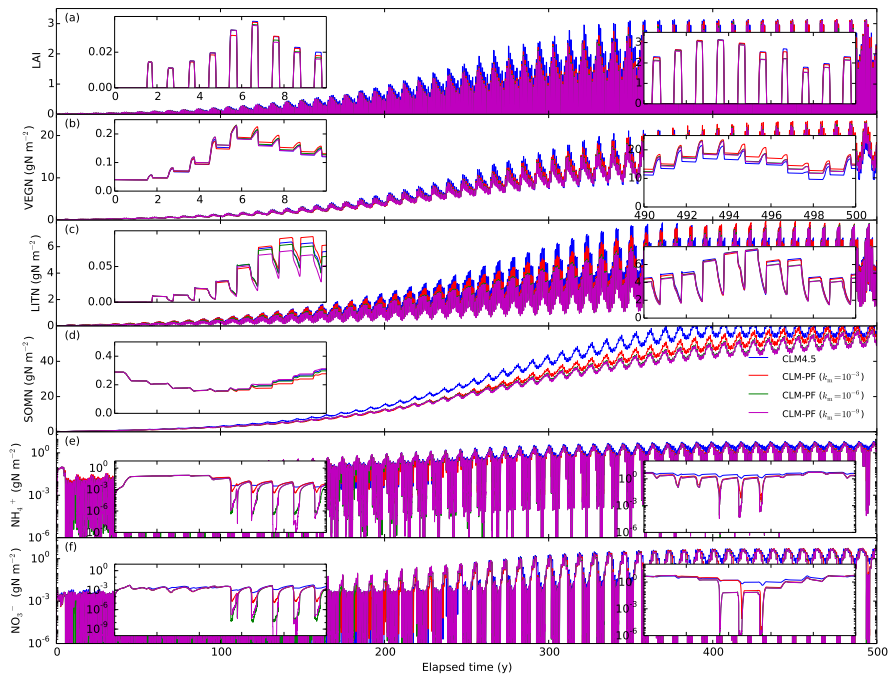


**Figure 7.** Calculated LAI and nitrogen distribution among vegetation, litter, SOM,  $\text{NH}_4^+$ , and  $\text{NO}_3^-$  pools in spin-up simulations for the US-Brw site. Log transformation is used to enforce nonnegativity for CLM-PFLTRAN.

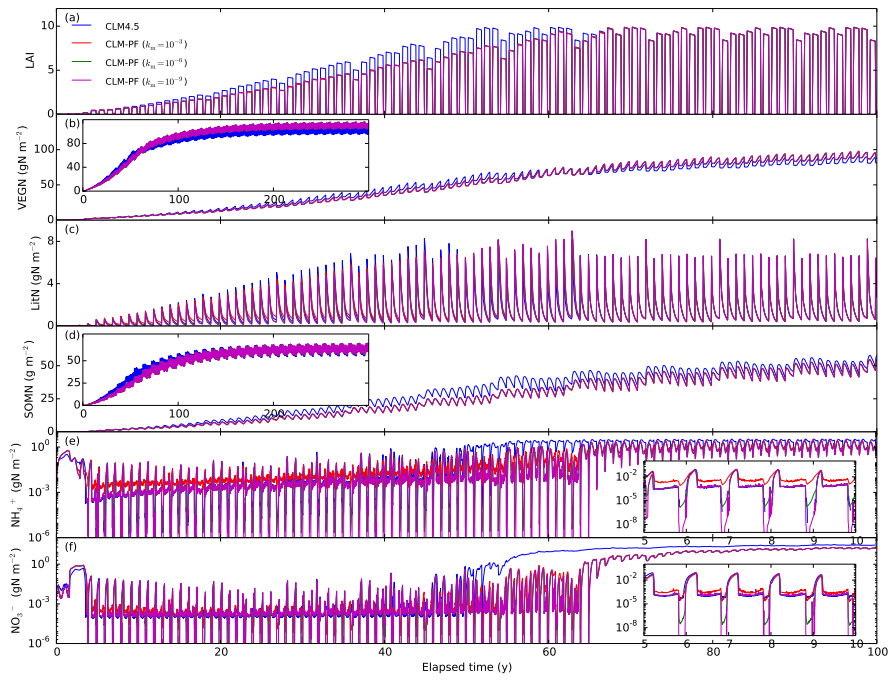


**Figure 8.** Calculated LAI and nitrogen distribution among vegetation, litter, SOM,  $\text{NH}_4^+$ , and  $\text{NO}_3^-$  pools in spin-up simulations for US-WBW site. Log transformation is used to enforce nonnegativity for CLM-PFLTRAN calculations.

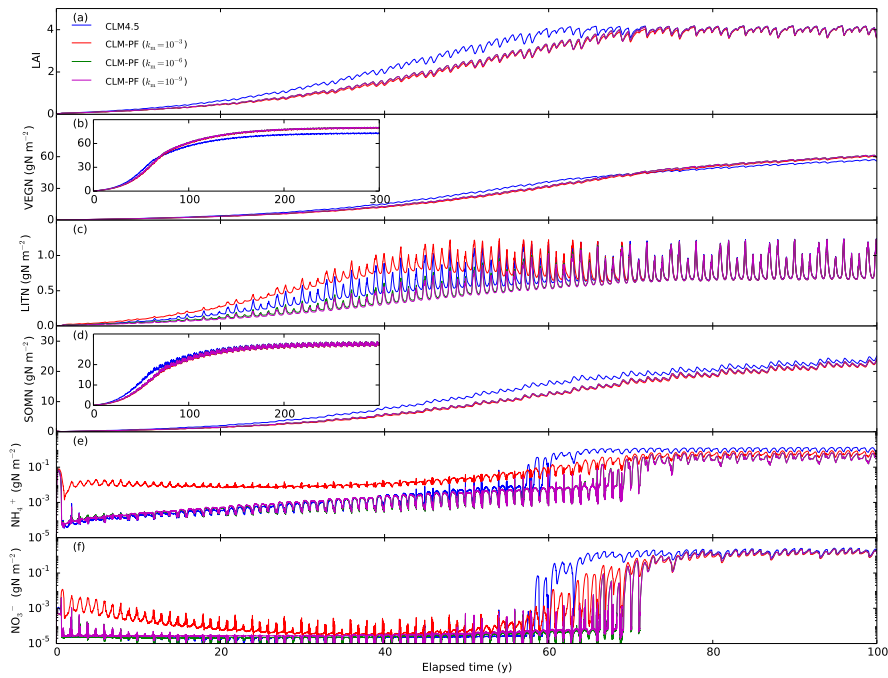


**Figure 9.** Calculated LAI and nitrogen distribution among vegetation, litter, SOM,  $\text{NH}_4^+$ , and  $\text{NO}_3^-$  pools in spin-up simulations for BR-Cax site. Log transformation is used to enforce nonnegativity for CLM-PFLOTRAN calculations.

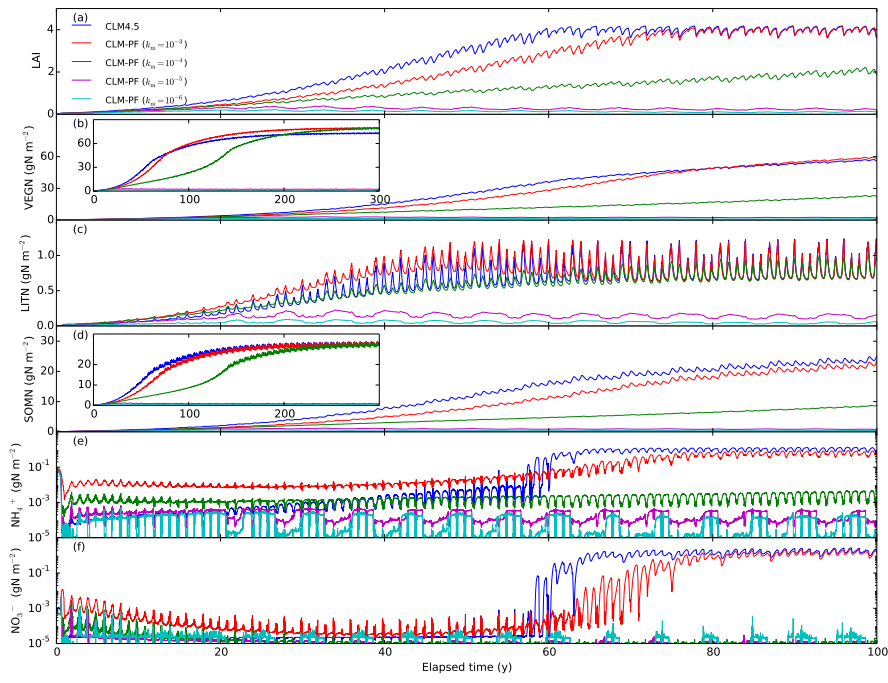


**Figure 10.** Calculated LAI and nitrogen distribution among vegetation, litter, SOM,  $\text{NH}_4^+$ , and  $\text{NO}_3^-$  pools in spin-up simulations for BR-Cax site. Scaling back update in each iteration is used enforce nonnegativity for CLM-PFLOTTRAN.

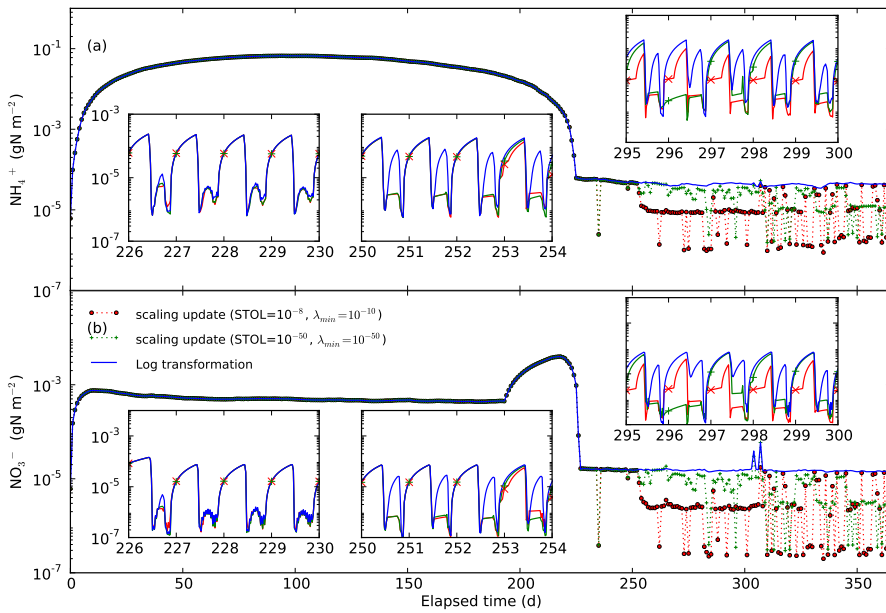


**Figure 11.** Calculated  $\text{NH}_4^+$  and  $\text{NO}_3^-$  concentration in the first year using SU (scaling update) vs. LT (log transformation) in the spin-up simulation for BR-Cax site with  $k_m = 10^{-6} \text{ mol m}^{-3}$ . “skip derivative” refers to not including the derivatives for the reaction (R11) with rate (Eq. A5) in the entries for  $\text{N}_2\text{Od}$  in the Jacobian matrix.

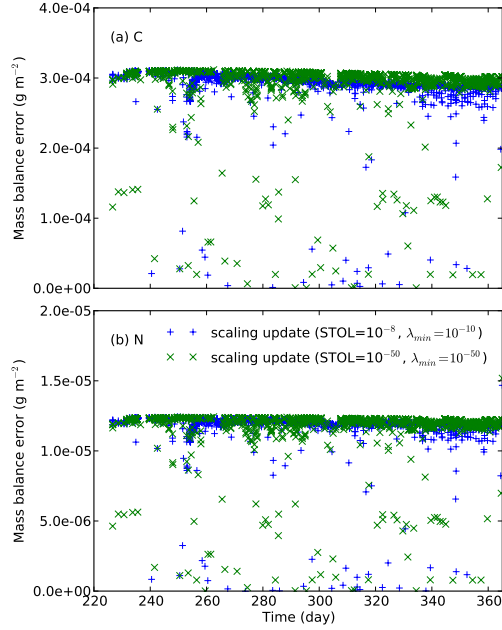


**Figure 12.** Mass balance error for (a) C and (b) N in the first year where SU with  $k_m = 10^{-6}$  mol m<sup>-3</sup> is used for the tropical site.

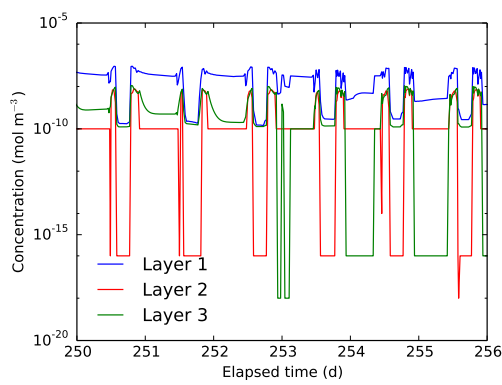


**Figure 13.** Diagnostic N<sub>2</sub>O concentration (N<sub>2</sub>Od from nitrification associated with net nitrogen mineralization Reaction R11 and rate Eq. A5) in the spin-up simulation for the BR-Cax site with  $k_m = 10^{-6}$  mol m<sup>-3</sup>. The concentration is reset to  $10^{-10}$  at the beginning of each CLM half hour time step. Scaling back update in each iteration is used to enforce nonnegativity.

**Table 1.** Wall time (hour) for spin-up simulation at the arctic, temperate, and tropical sites on OIC

Site	CLM	SU ( $10^{-3}$ )	SU ( $10^{-6}$ )	SU ( $10^{-9}$ )	LT ( $10^{-3}$ )	LT ( $10^{-6}$ )	LT ( $10^{-9}$ )	LT ( $10^{-12}$ )
DC								
US-Brw	18.1	24.8	25.5	29.2	38.5	40.8	47.0	49.5
US-Pit	11.7	17.1	14.8	14.9	30.0	37.5	40.2	43.1
BR-Cax	10.9	16.2	18.6	18.0	40.2	40.5	45.7	52.0
DR								
US-Brw	18.1	21.5	21.5		35.8	35.9		
US-Pit	11.7	14.1	14.1		26.9	26.7		
BR-Cax	10.9	16.4	16.4		42.2	41.6		

SU = scaling update, LT = log transformation,  $10^{-3}$ ,  $10^{-6}$ , and  $10^{-9}$  are  $k_m$ , DC and DR = downregulating consumption as a function of concentration and rate, OIC = ORNL Institutional Cluster (Phase5), US-Brw simulation duration = 500 year and US-Pit and BR-Cax simulation duration = 300 year. For the last column LT ( $10^{-12}$ ), MAX\_CUT is increased from default 16 to 50.

## Appendix A: CLM biogeochemical reactions and rates

### A1 CLM-CN decomposition

The CLM-CN decomposition cascade consists of three litter pools with variable CN ratios, four soil organic matter (SOM) pools with constant CN ratios, and seven reactions (Fig. 1A). The reaction

920 can be described by



with  $\text{CN}_u$  and  $\text{CN}_d$  as the upstream and downstream pool (molecular formula, for 1 mol upstream and downstream pool, there is  $u$  and  $d$  mol N),  $N$  as either  $\text{NH}_4^+$  or  $\text{NO}_3^-$ ,  $f$  as the respiration fraction, and  $n = u - (1 - f)d$ . The rate is

$$925 \quad \frac{d[\text{CN}_u]}{dt} = -k_d f_T f_w [\text{CN}_u], \quad (\text{A1})$$

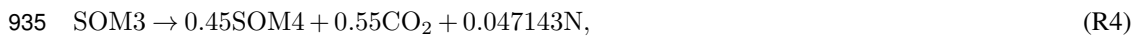
with  $k_d$  as the rate coefficient and  $f_T$  and  $f_w$  as the temperature and moisture response functions,

$$f_T = Q_{10}^{(T-25)/10}, \quad (\text{A2})$$

and

$$f_w = \ln(\psi) Q_{10}^{(T-25)/10}, \quad (\text{A3})$$

930 With a constant CN ratio, the decomposition reactions for the four SOM pools are



and



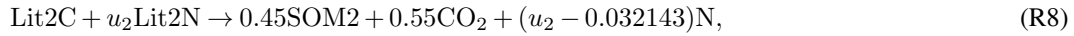
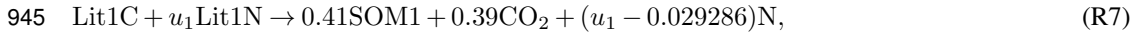
The exact stoichiometric coefficients are calculated in the code using values for respiration factor, CN ratio, and molecular weight specified in the input file.

940 CLM4.5 has an option to separate N into  $\text{NH}_4^+$  and  $\text{NO}_3^-$ . The N mineralization product is  $\text{NH}_4^+$ .

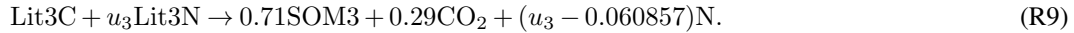
As the CN ratio is variable for the three litter pools, litter N pools need to be tracked such that reaction (R1) becomes



with  $u = [\text{LitN}]/[\text{LitC}]$ . The three litter decomposition reactions are



and



950 As the CN ratio of the litter pools is generally high,  $u_1$ ,  $u_2$ , and  $u_3$  are usually small, and  $n$  in these reactions (e.g.,  $n_1 = u_1 - 0.029286$  for Lit1) is normally negative. Namely, these reactions consume (immobilize) N, which can be  $\text{NH}_4^+$ ,  $\text{NO}_3^-$ , or both.

## A2 Nitrification

The nitrification reaction to produce  $\text{NO}_3^-$  is



with  $\dots$  for additional reactants and products to balance the reaction. The rate is (Dickinson et al., 2002)

$$\frac{d[\text{NH}_4^+]}{dt} = -\frac{d[\text{NO}_3^-]}{dt} = -k_n f_T f_w [\text{NH}_4^+]. \quad (\text{A4})$$

The nitrification reaction to produce  $\text{N}_2\text{O}$  is



with one component related to decomposition as

$$\frac{d[\text{NH}_4^+]}{dt} = -2 \frac{d[\text{N}_2\text{O}]}{dt} = -f_{nm} f_T f_w f_{pH} \max(R_{nm}, 0) \quad (\text{A5})$$

with  $f_{nm}$  as a fraction (Parton et al., 1996) and  $R_{nm}$  as the net N mineralization rate,

$$R_{nm} = \sum_i n_i R_i, \quad (\text{A6})$$

965 where  $R_i$  denotes the rate of reaction (R2, R3, R4, R5, R7, R8, R9). The second component is (Parton et al., 1996)

$$\frac{d[\text{NH}_4^+]}{dt} = -2 \frac{d[\text{N}_2\text{O}]}{dt} = -k_{n2o} f_T f_w f_{pH} (1 - e^{-0.0105[\text{NH}_4^+]}) \quad (\text{A7})$$

Ignoring the high-order terms and moving the unit conversion factor into  $k_{n2o}$ , it can be simplified as a first-order rate as

970  $\frac{d[\text{NH}_4^+]}{dt} = -2 \frac{d[\text{N}_2\text{O}]}{dt} = -k_{n2o} f_T f_w f_{pH} [\text{NH}_4^+]$ . (A8)

### A3 Denitrification

The denitrification reaction is



with rate (Dickinson et al., 2002)

$$975 \quad \frac{d[\text{NO}_3^-]}{dt} = -2 \frac{d[\text{N}_2]}{dt} = -k_{\text{deni}} f_T f_w f_{\text{pH}} [\text{NO}_3^-]. \quad (\text{A9})$$

### A4 Plant nitrogen uptake

The plant nitrogen uptake reaction can be written as



and



The rate is specified by CLM (plant nitrogen demand) and assumed to be constant in each half-hour time step.

### A5 Demand-based competition and distributing nitrogen demand between $\text{NH}_4^+$ and $\text{NO}_3^-$

Denote  $R_{d,p}$ ,  $R_{d,i}$ ,  $R_{d,nitr}$ ,  $R_{d,deni}$  as the potential plant, immobilization, nitrification, and denitrification demand (rate);  $R_{a,tot} = R_{d,p} + R_{d,i} + R_{d,nitr}$  as the total  $\text{NH}_4^+$  demand; and  $R_{n,tot}$  as the total  $\text{NO}_3^-$  demand. CLM uses a demand-based competition approach to split the available sources in proportion to the demand rates to meet the demands (Oleson et al., 2013; Thornton and Rosenbloom, 2005). Specifically, for each time step, if  $R_{a,tot}\Delta t \leq [\text{NH}_4^+]$ , the uptakes are equal to potential demands, and  $R_{n,tot} = 0$ ; otherwise, the uptakes for  $\text{NH}_4^+$  are  $[\text{NH}_4^+]R_{d,p}/R_{a,tot}\Delta t$ ,  $985 \quad [\text{NH}_4^+]R_{d,i}/R_{a,tot}\Delta t$ , and  $[\text{NH}_4^+]R_{d,nitr}/R_{a,tot}\Delta t$  for plants, immobilization, and nitrification, respectively;  $R_{n,tot} = R_{a,tot} - [\text{NH}_4^+]/\Delta t + R_{d,deni}$ . If  $R_{n,tot}\Delta t < [\text{NO}_3^-]$ , all of the remaining demand  $R_{n,tot}$  is met with available  $\text{NO}_3^-$ . Otherwise, available  $\text{NO}_3^-$  is split to meet the remaining plant, immobilization, and denitrification demands in proportion to their rates.

### Appendix B: Downregulation with cutoff

995 An alternative to using a residual concentration (Eq. 16) is to introduce a cutoff, e.g., Eq. (A1) becomes

$$\frac{d[\text{CN}_u]}{dt} = -k_d f_T f_w [\text{CN}_u] f([\text{CN}_u]), \quad (\text{B1})$$

with  $f([CN_u]) = 1$  when  $[CN_u] \geq [CN_u]_r$ , and 0 otherwise. It is simple but does not prevent  $[CN_u]$  from getting below  $[CN_u]_r$  or 0 in theory. In addition, it introduces a discontinuity. A polynomial function can be used to smooth the cutoff

$$f([CN_u]) = 1 - \left[ 1 - \left( \frac{[CN_u] - [CN_u]_r}{[CN_u]_1 - [CN_u]_r} \right)^2 \right]^2. \quad (B2)$$

This function varies from 0 at  $[CN_u]_r$  to 1 at  $[CN_u]_1$ , with zero derivatives at both points. While not implying a nonphysical reverse reaction as Eq. (16),

$$\frac{df([CN_u])}{d[CN_u]} = 4 \frac{[CN_u] - [CN_u]_r}{([CN_u]_1 - [CN_u]_r)^2} \left[ 1 - \left( \frac{[CN_u] - [CN_u]_r}{[CN_u]_1 - [CN_u]_r} \right)^2 \right]. \quad (B3)$$

Depending on  $[CN_u]_1 - [CN_u]_r$ , this cutoff does introduce a large derivative change during the transition:  $df([CN_u])/d[CN_u]$  varies from 0 to  $10^8$  for  $[CN_u]_r=10^{-10}$  and  $[CN_u]_1=10^{-8}$  (Fig. 14). The maximum increases at about the same order of magnitude as the decrease of  $[CN_u]_r$  and  $[CN_u]_1$ . Even though smoothed, the cutoff is still a sharp change. The smaller the cutoff concentrations, the sharper the transitions. Marching through a steep transition in time usually involves small time steps.

1010

### Appendix C: Downregulation of consumption as a function of rates

The contribution of  $n$  reactions to the rate component in the residual and Jacobian for species  $i$  are

$$\mathbf{R}(i) = \sum_{j=1}^n \nu_{ij} R_j, \quad (C1)$$

and

$$1015 \quad \mathbf{J}(i, k) = \frac{\partial \mathbf{R}(i)}{\partial \mathbf{C}(k)} = \sum_{j=1}^n \frac{\partial (\nu_{ij} R_j)}{\partial \mathbf{C}(k)}, \quad (C2)$$

with  $\mathbf{C}$  as the concentration vector,  $\mathbf{R}$  as the rate vector,  $\mathbf{J}$  as the component of Jacobian matrix ( $m$  by  $m$ ) that is associated with  $\mathbf{R}$ ,  $\nu_{ij}$  as stoichiometric coefficient of species  $i$  in reaction  $j$  ( $\sum_{i=1}^m \nu_{ij} \mathbf{C}(i) = 0$ ), and  $R_j$  as the rate of reaction  $j$ , a function of the activities (concentration) of the reactants, products, and environmental variables (moisture, temperature, pH, redox, etc.).

#### 1020 C1 Downregulation of consumption for one species

Depending on whether a species  $a$  (e.g.,  $\text{NH}_4^+$ ) is a reactant ( $\nu_{aj} > 0$ ) or a product ( $\nu_{aj} < 0$ ), we divide the  $n$  reactions into a demand (subscript  $da$  for demand  $a$ ) and a supply (subscript  $sa$  for supply  $a$ ) group:

$$R_{da} = \sum_{j=1}^{n_{da}} \nu_{da,aj} R_{da,j}, \quad (C3)$$

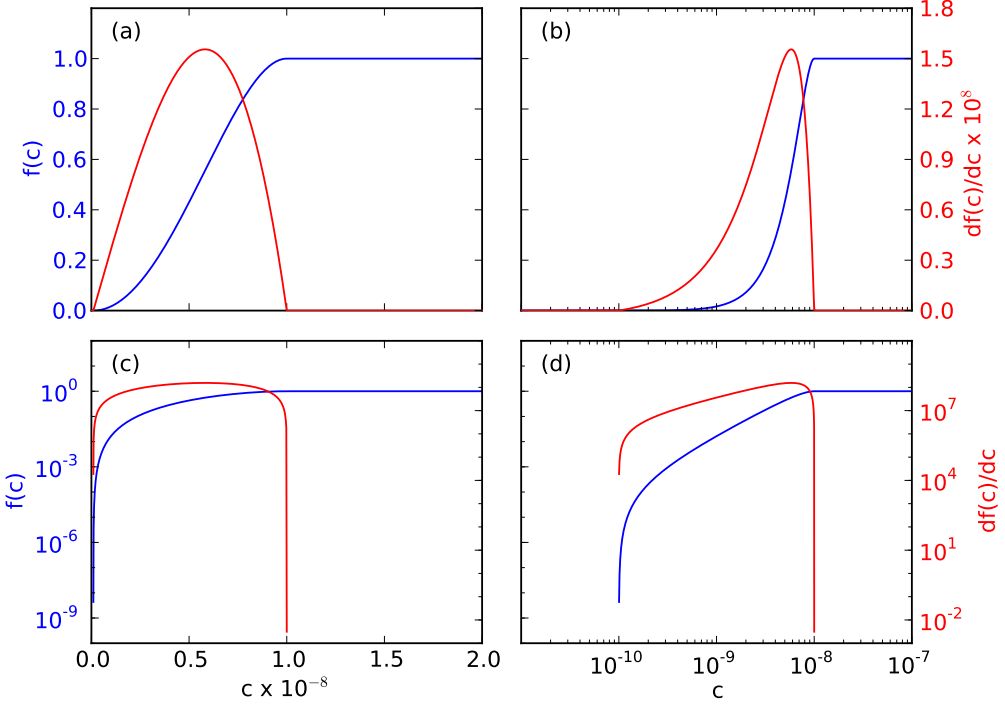


**Figure 14.** Smoothed cutoff function (Eq. B2) and derivative (Eq. B3). The y axis is in log in (c) and (d), while the x axis is in log in (b) and (d). Even though smoothed, the cutoff is a steep transition. The derivative varies by orders of magnitude in a small concentration range and requires small time step size to march through.

1025 and

$$R_{sa} = \sum_{j=1}^{n_{sa}} \nu_{sa,aj} R_{sa,j}, \quad (C4)$$

with  $n_{da}$  as the number of reactions that consume species  $a$ ,  $\nu_{da,aj}$  as the stoichiometric coefficient of species  $i$  in  $a$  consuming reaction  $j$ ,  $n_{sa}$  as the number of reactions that produce species  $a$ ,  $\nu_{sa,ij}$  as the stoichiometric coefficient of species  $i$  in a producing reaction  $j$ ,  $R_{da}$  as  $a$  consumption (demand) rate ( $\text{mol s}^{-1}$ , negative), and  $R_{sa}$  as  $a$  production (supply) rate ( $\text{mol s}^{-1}$ , positive). Therefore,

$$\mathbf{R}(i) = \sum_{j=1}^{n_{sa}} \nu_{sa,aj} R_{sa,j} + \sum_{j=1}^{n_{da}} \nu_{da,aj} R_{da,j} = \mathbf{R}_{sa}(i) + \mathbf{R}_{da}(i), \quad (C5)$$

and

$$\mathbf{J}(i, k) = \frac{\partial \mathbf{R}(i)}{\partial \mathbf{C}(k)} = \sum_{j=1}^n \frac{\partial(\nu_{ij} R_j)}{\partial \mathbf{C}(k)} = \sum_{j=1}^{n_{sa}} \frac{\partial(\nu_{sa,ij} R_{sa,j})}{\partial \mathbf{C}(k)} + \sum_{j=1}^{n_{da}} \frac{\partial(\nu_{da,ij} R_{da,j})}{\partial \mathbf{C}(k)} = \mathbf{J}_{sa} + \mathbf{J}_{da}. \quad (C6)$$

Define a downregulation factor

$$1035 \quad d_a = \min \left( 1, -\frac{R_{sa} \Delta t + [\mathbf{C}(a) - \epsilon] V}{R_{da} \Delta t} \right) = \min \left( 1, -\frac{s_a}{D_a} \right), \quad (C7)$$

with  $V$  as the bulk volume or volume of liquid water of the grid cell for species with concentration unit  $\text{mol m}^{-3}$  or M. After downregulation,

$$\mathbf{R}_a = \mathbf{R}_{sa} + d_a \mathbf{R}_{da}, \quad (\text{C8})$$

1040  $\mathbf{J}_a(i, k) = \frac{\partial \mathbf{R}_a(i)}{\partial \mathbf{C}(k)} = \mathbf{J}_{sa}(i, k) + d_a \mathbf{J}_{da}(i, k) + \mathbf{R}_{da}(i) \frac{\partial d_a}{\partial \mathbf{C}(k)}, \quad (\text{C9})$

$$\frac{\partial d_a}{\partial \mathbf{C}(k)} = - \left( \frac{\partial s_a}{\partial \mathbf{C}(k)} D_a - s_a \frac{\partial D_a}{\partial \mathbf{C}(k)} \right) D_a^{-2}, \quad (\text{C10})$$

1045  $\frac{\partial s_a}{\partial \mathbf{C}(a)} = \sum_{j=1}^{n_{sa}} \frac{\partial (\nu_{sa,aj} R_{sa,j})}{\partial \mathbf{C}(a)} \Delta t + V, \quad (\text{C11})$

$$\frac{\partial s_a}{\partial \mathbf{C}(k)} = \sum_{j=1}^{n_{sa}} \frac{\partial (\nu_{sa,kj} R_{sa,j})}{\partial \mathbf{C}(k)} \Delta t, \quad (\text{C12})$$

$$\frac{\partial D_a}{\partial \mathbf{C}(k)} = \sum_{j=1}^{n_{da}} \frac{\partial (\nu_{da,kj} R_{da,j})}{\partial \mathbf{C}(k)} \Delta t, \quad (\text{C13})$$

Implementation in PFLOTTRAN involves 1) adding variables  $\mathbf{R}_{sa}$ ,  $\mathbf{R}_{da}$ , and  $\mathbf{J}_a$ , 2) accumulating the values in each reaction rate formula, and 3) conducting downregulation and adding the contribution to the global residual vector and Jacobian matrix.

## C2 Downregulation of consumption for a second species

In addition to species  $a$  (e.g.,  $\text{NH}_4^+$ ), we want to downregulate another species  $l$ , for example,  $\text{NO}_3^-$ .

The treatment is the same except for the reactions that consume species  $a$  and produce species  $l$ .

1055 Suppose we have a nitrification reaction (R10) with rate  $R_{al}$ , and  $R'_{al} = dR_{al}/d[\text{NH}_4^+]$ . The rate and derivative are added in demand rate and derivative for  $\text{NH}_4^+$  ( $\mathbf{R}_{sa}$ ,  $\mathbf{R}_{da}$ ,  $\mathbf{J}_{sa}$ ,  $\mathbf{J}_{da}$ ), not in the sink rate and derivative for  $\text{NO}_3^-$  ( $\mathbf{R}_{sl}$ ,  $\mathbf{R}_{dl}$ ,  $\mathbf{J}_{sl}$ ,  $\mathbf{J}_{dl}$ ). Define a downregulation factor

$$d_l = \min \left( 1, - \frac{R_{sl} \Delta t + (\mathbf{C}(l) - \epsilon) V_w + R_{al} d_a \Delta t}{R_{dl} \Delta t} \right) = \min(1, - \frac{s_l}{D_l}), \quad (\text{C14})$$

1060  $\mathbf{R}_l = \mathbf{R}_{sl} + d_l \mathbf{R}_{dl}, \quad (\text{C15})$

$$\mathbf{J}_l(i, k) = \frac{\partial \mathbf{R}_l(i)}{\partial \mathbf{C}(k)} = \mathbf{J}_{sl}(i, k) + d_l \mathbf{J}_{dl}(i, k) + \mathbf{R}_{dl}(i) \frac{\partial d_l}{\partial \mathbf{C}(k)}, \quad (\text{C16})$$

$$\frac{\partial d_l}{\partial \mathbf{C}(k)} = - \left( \frac{\partial s_l}{\partial \mathbf{C}(k)} D_l - s_l \frac{\partial D_l}{\partial \mathbf{C}(k)} \right) D_l^{-2}, \quad (C17)$$

1065

$$\frac{\partial s_l}{\partial \mathbf{C}(l)} = \sum_{j=1}^{n_{sl}} \frac{\partial (\nu_{sl,lj} R_{sl,j})}{\partial \mathbf{C}(l)} \Delta t + V_w + \underline{\frac{\partial (R_{al} d_a)}{\partial \mathbf{C}(l)}}, \quad (C18)$$

$$\frac{\partial s_l}{\partial \mathbf{C}(k)} = \sum_{j=1}^{n_{sl}} \frac{\partial (\nu_{sl,kj} R_{sl,j})}{\partial \mathbf{C}(k)} \Delta t + \underline{\frac{\partial (R_{al} d_a)}{\partial \mathbf{C}(K)}}, \quad (C19)$$

and

$$1070 \quad \frac{\partial D_a}{\partial \mathbf{C}(k)} = \sum_{j=1}^{n_{da}} \frac{\partial (\nu_{da,kj} R_{da,j})}{\partial \mathbf{C}(k)} \Delta t. \quad (C20)$$

In addition to variables  $\mathbf{R}_{sl}$ ,  $\mathbf{R}_{dl}$ , and  $\mathbf{J}_l$ , downregulating the second species requires two additional variables,  $R_{al}$ , and  $R'_{al}$ . When accumulating the values in each reaction rate formula, the production rate from the reaction that consumes the first species has to be carefully treated as it is downregulated for the first species. Conducting downregulation involves additional terms, as underlined in the equations. Compared with the downregulation for the first species, downregulating the second species that can be produced from the first species with a simple  $A \rightarrow B$  reaction becomes much more complicated. If we add another reaction that consumes the second species to produce the first species, this approach has to be modified.

1075 In general, many if not all species need to be downregulated. Extending this approach involves adding many variables (vectors and matrices) to track the consumption and production rates and their derivatives. The consumption and production relationship among many species can be complicated, making generalization of this approach challenging if not infeasible.

## Appendix D: A semi-analytical solution for Monod equation

As an analytical solution is not available, discretizing Eq. (22) using the backward Euler method, it 1085 becomes

$$[\text{NH}_4^+]^{k+1} + (k_m + R_a \Delta t - [\text{NH}_4^+]^k) [\text{NH}_4^+]^{k+1} - k_m [\text{NH}_4^+]^k = 0. \quad (D1)$$

The two roots are

$$[\text{NH}_4^+]^{k+1} = 0.5 \left[ [\text{NH}_4^+]^k - k_m - R_a \Delta t \pm \sqrt{([\text{NH}_4^+]^k - k_m - R_a \Delta t)^2 + 4k_m [\text{NH}_4^+]^k} \right]. \quad (D2)$$

## Appendix E: Matrix equation for example Test 2

$$1090 \quad \begin{bmatrix} \frac{1}{\Delta t} + J_{at} + J_{nitr} & 0 & 0 \\ -J_{at} & \frac{1}{\Delta t} & 0 \\ -J_{nitr} & 0 & \frac{1}{\Delta t} \end{bmatrix} \begin{pmatrix} \delta[\text{NH}_4^+]^{k+1,1} \\ \delta[\text{PlantA}]^{k+1,1} \\ \delta[\text{NO}_3^-]^{k+1,1} \end{pmatrix} = \begin{pmatrix} R_{at} + R_{nitr} \\ -R_{at} \\ -R_{nitr} \end{pmatrix}. \quad (E1)$$

## Appendix F: Matrix equation for example Test 3

$$\begin{bmatrix} \frac{1}{\Delta t} + J_{at} + J_{nitr} & 0 & 0 & 0 & 0 \\ -J_{at} & \frac{1}{\Delta t} & 0 & 0 & 0 \\ -J_{nitr} + J_{nt,a} & 0 & \frac{1}{\Delta t} + J_{nt} + J_{deni} & 0 & 0 \\ -J_{nt,a} & 0 & -J_{nt,n} & 1/\Delta t & 0 \\ 0 & 0 & -0.5J_{deni} & 0 & 1/\Delta t \end{bmatrix} \begin{pmatrix} \delta[\text{NH}_4^+]^{k+1,1} \\ \delta[\text{PlantA}]^{k+1,1} \\ \delta[\text{NO}_3^-]^{k+1,1} \\ \delta[\text{PlantN}]^{k+1,1} \\ \delta[\text{N}_2]^{k+1,1} \end{pmatrix} = \begin{pmatrix} R_{at} + R_{nitr} \\ -R_{at} \\ -R_{nitr} + R_{nt} + R_{deni} \\ -R_{nt} \\ -0.5R_{deni} \end{pmatrix}. \quad (\text{F1})$$

## Appendix G: Supplemental figures

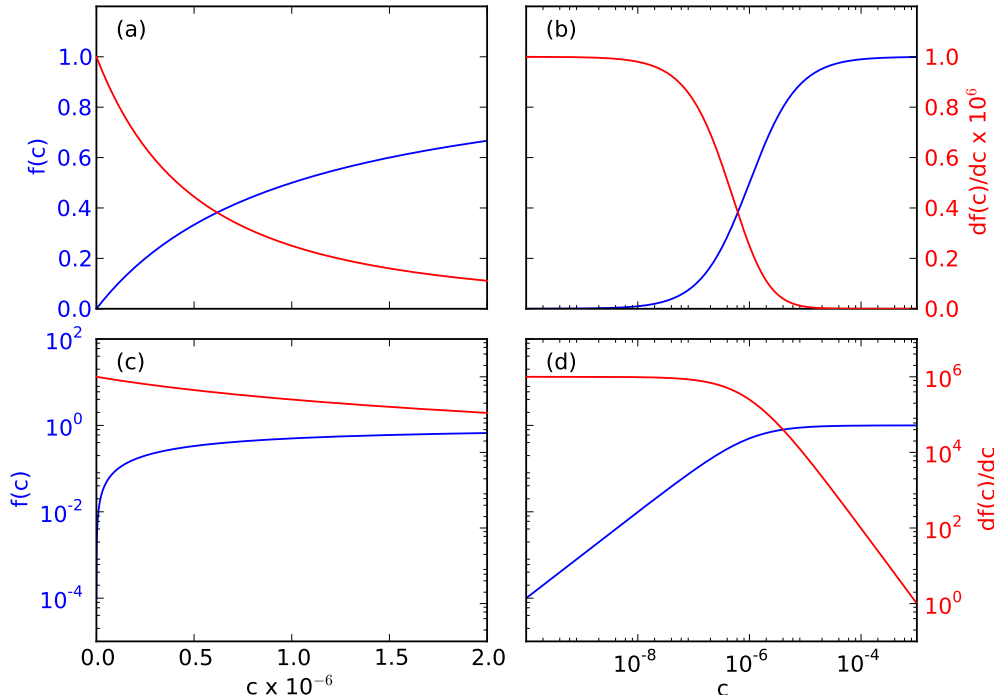


**Figure 15.** Monod substrate limiting function (Eq. 18) and derivative. The y axis is in log in (c) and (d), while the x axis is in log in (b) and (d). As the function switches from zero-order to first-order, the derivative jumps six ( $k_m^{-1}$ ) orders of magnitudes, requiring small time step size to step through.

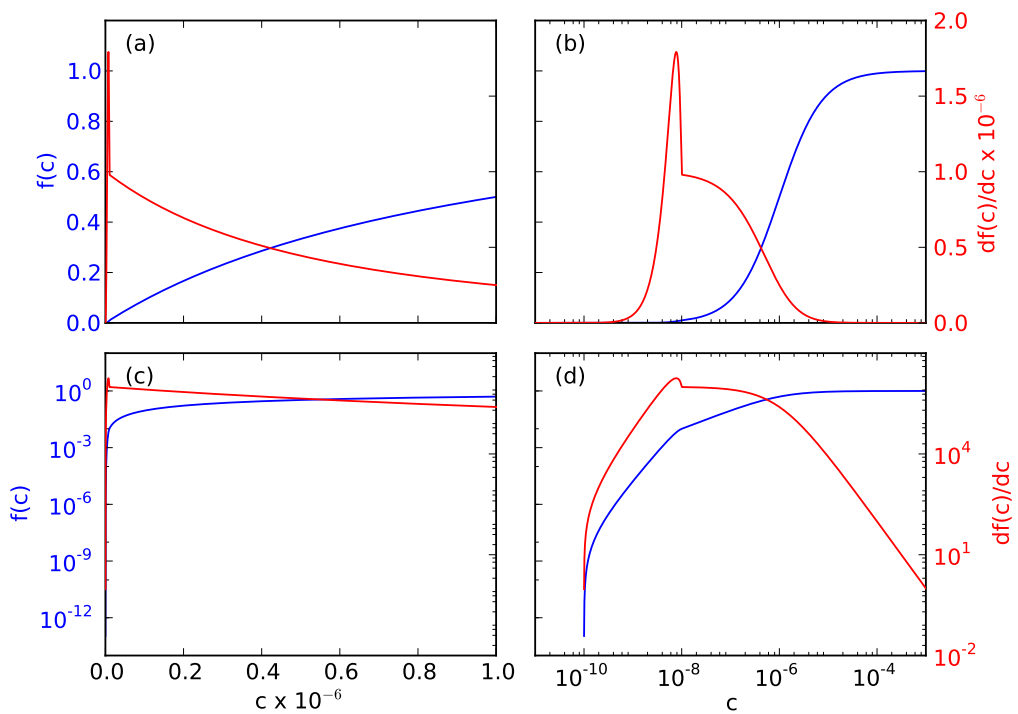


**Figure 16.** A combination of the Monod substrate limiting function (Eq. 18, Fig. 15) and the smoothed cutoff function (Eq. B2, Fig. 14) introduces steep transitions that require small time step sizes to march through.